

CORAL

A Cosmic Ray experiment in and above the LHC tunnel

V. Avati, L. Dick^{o)}, K. Eggert^{*)}, A. Zinchenko^{a)}
CERN, Geneva, Switzerland

C. Taylor
Case Western Reserve University, Cleveland, OH, USA

E. Casimiro Linares, A. Zepeda
Cinvestav-IPN, Mexico City, Mexico

R. Orava, M. Karhunen, J. Ström^{b)}
Helsinki Institute of Physics, Helsinki, Finland

S. Akimenko, V. Ronjin, V. Tikhonov, E. Vlassov,
IHEP, Institute for High Energy Physics, Protvino, Russia

V. Berezinsky, F. Vissani
Laboratori Nazionali del Gran Sasso and INFN, Italy

L. Jones
University of Michigan, MI, USA

S.K. Gupta, A. Jain, K.C. Ravindran, S.C. Tonwar and K. Viswanathan
Tata Institute of Fundamental Research, Mumbai, India

Y. Hayashi, S. Kawakami, T. Yoshikoshi
Osaka City University, Osaka, Japan

J. Kangas, J. Peltoniemi, M. Vallinkoski
University of Oulu and Sodankylä Geophysical Observatory, Finland

J. Ridky, P. Travnicek
FzU, Institute of Physics of the C.A.S. High Energy Physics Division,
Prague, Czech Republic

D. Nosek
IPNP, Institute of Particle and Nuclear Physics, Faculty of Mathematics and Physics,
Charles University, Prague, Czech Republic

A. Fernandez, E. Gamez, R. Lopez, S. Roman
Universidad Autonoma de Puebla, FCFM-UAP, Puebla, Mexico

A. Karjalainen, M. Korhonen, A. Mattila, N. Patrikainen, J. Pennanen, M. Rahkala
Rovaniemi Polytechnic, Rovaniemi, Finland

C. Grupen, A. Mailov^{c)}
University of Siegen , Siegen, Germany

I. Kirov, J. Stamenov, S. Ushev, Hr. Vankov
Institute for Nuclear Research and Nuclear Institute, Sofia, Bulgaria

N. Shivarov, B. Stojanov, R. Zahariev
Central Laboratory of Mechatronics and Instrumentation, Bulgarian Academy of Sciences,
Sofia, Bulgaria

J. Strauss
Institute for High Energy Physics, Vienna, Austria

A. Akhperjanian, Y. Margaryan, L. Pogossyan, V. Sahakian
Yerevan Physics Institute, Yerevan, Armenia

Abstract

The CORAL collaboration proposes a cosmic ray experiment consisting of an array of muon tracking chambers in the underground cavern at PA4 together with an array of scintillation counters on the surface above. This location is ideal for both the underground muon array and the surface air shower array.

CORAL will provide unique data on multi-muon production in cosmic ray air showers in a particularly interesting energy regime. Together with the simultaneous and complementary measurement of the electromagnetic structure of the air showers, CORAL will

- determine the composition of cosmic ray primaries with unprecedented precision over the energy range 10^{14} eV to a few times 10^{16} eV
- provide a sensitive instrument for the study of the structure of cosmic ray air showers, including anomalies such as those suggest by Centauro and anti-Centauro events
- significantly extend the study of the high multiplicity muon excess previously observed with the ALEPH detector.

CORAL is an economical experiment, inheriting the complete air shower array from the HEGRA experiment, as well as muon drift chambers and scintillation trigger counters from UA1, DELPHI and OPAL. While LHC construction work at PA4 imposes constraints on the experiment, no major difficulties are foreseen.

^{o)} retired from CERN

^{*}) Contact person

^{a)} visitor from Joint Institute for Nuclear Research (JINR), Dubna, Russia

^{b)} visitor from ARCADA Polytechnic, Helsinki, Finland

^{c)} on leave from Baku University, Azerbaijan

Contents

1	Physics Goals	1
1.1	<i>Overview</i>	1
1.2	<i>Cosmic Ray Experiments with large underground detectors at CERN</i>	2
1.3	<i>The cosmic ray spectrum</i>	3
1.4	<i>Muons in air showers</i>	3
1.5	<i>Underground muon experiments</i>	5
1.6	<i>Cosmic Ray Results Obtained with the ALEPH Detector</i>	6
1.7	<i>Capabilities of the CORAL Detector</i>	11
1.8	<i>Other Possible Surprises</i>	11
1.9	<i>Muon Astronomy</i>	13
2	Results from the test set-up in the underground area at BA4	15
2.1	<i>Performance of UA1 and DELPHI Chambers</i>	15
2.2	<i>Reconstruction of multi-muon events</i>	19
3	The experimental Set-up	24
3.1	<i>The underground muon array</i>	24
3.2	<i>The surface air shower array</i>	25
3.3	<i>Trigger</i>	32
4	Monte Carlo studies of detector performance	36
4.1	<i>The CORSIKA Monte-Carlo</i>	36
4.2	<i>The underground muon array alone</i>	36
4.3	<i>Combined air shower and underground muon array</i>	39
5	Schedule	47
6	Budget	48
A	Calculation of the muon momentum cut-off	50

1 Physics Goals

The CORAL Collaboration proposes to install a 21 x 23 m² array of muon tracking chambers in the underground cavern at PA4 (the former ALEPH experimental region), together with a 150 x 150 m² array of scintillation counters arranged on a 10 m grid on the surface above PA4. The simultaneous and complementary measurement of the muonic and the electromagnetic component of a cosmic ray air shower with this apparatus will provide the determination of both shower core and primary energy by two independent methods. The CORAL detector will also be a sensitive instrument for the study of fluctuations in the charged-to-neutral distribution of cosmic rays, such suggested by theoretical models such as Disoriented Chiral Condensates, and by observations of Centauro and AntiCentauro events. CORAL will also determine the primary particle species with an unprecedented precision for primary energies from 10¹⁴ eV to a few times 10¹⁶ eV.

This proposal thus represents a significant extension of the capabilities of the earlier CosmoLep proposal [1] for an underground muon array alone.

An important part of the CORAL experimental program is the further study of the high-multiplicity muon excess previously observed with the ALEPH detector. The large underground tracking detectors with good multi-particle resolution will provide information on the size, structure, and radial profile of high-multiplicity muon events, and will also discriminate against muon induced showers from the rock overburden which might mimic high-multiplicity events. This information from the underground muon array can then be correlated with detailed information about the electromagnetic component of the shower provided by the surface array. CORAL will collect much larger data sets and will thus dramatically improve both the statistics and the characterization of these anomalous events.

1.1 Overview

In recent decades, cosmic ray air showers initiated by high-energy proton or nucleus collisions in the atmosphere have been studied with large area experiments on the surface or with muon measurements deep underground. In principle, these cosmic ray experiments explore two completely different realms of physics, particle astrophysics and particle interaction physics, which are, however, intimately related by the interpretation of the data.

The precise measurement of the cosmic ray energy spectrum and, in particular, of the chemical composition of cosmic ray primaries in the vicinity of the “knee” (10¹⁵ eV to 10¹⁷ eV) may shed light on the origin of cosmic rays and hence on their acceleration mechanism. This composition is precisely known from direct measurements in satellites and balloon experiments only for energies below 10¹⁴ eV, due to rate limitations. Higher energies must be studied by large detector areas on the surface or underground.

The determination of the primary particle species from ground level observables depends critically on the detailed understanding of the interaction mechanism of the showering particles with air. Particle production, both at large energies and in the forward direction, can today only be estimated by model based extrapolation of accelerator data. Indeed, there are no accelerator data for particle production at very small forward angles and in the relevant energy region around the “knee”. In fact, new phenomena in very forward high-energy hadronic interactions, such as coherent pion production, disoriented chiral condensate states or heavy flavour production can significantly influence the hadronic cascade and hence the observables at the ground level. This may be the cause for the conflicting results about the particle composition among various experiments which have not been satisfactorily resolved.

The interpretation of the cosmic ray data depends crucially on models extrapolated well be-

yond the range in which they have been tuned or tested. While it may be that some of the models will converge on a common interpretation, they may still be incorrect. Hence, the greater the diversity of the measurements which the models must confront, the greater the likelihood of converging to the correct answer. As many complementary measurements as possible should be made in order to understand more about the forward particle production and hence about the cosmic spectrum, and to provide cross-checks on the interpretation of the results.

Cosmic ray air showers are characterized by the distribution of the electromagnetic and muonic components at ground level and by muon distributions at different underground levels. In this proposal we want to stress the importance of correlations between the electromagnetic component at ground level and detailed muon measurements at a modest depth of 140 m underground. At these depths, the electromagnetic and hadronic components of the air showers are fully absorbed, and the muon momentum cut-off is about 70 GeV.

This is in contrast to experiments deep underground, such as MACRO [2], SuperKamiokande [3], IMB [4], and Frejus [5, 6] where the cutoff is of the order of one TeV, as well as to surface experiments such as KASCADE [7], AGASA [8], CASA-MIA [9] and GRAPES [10], where the cut-off is of the order of one or two GeV. Cosmic ray experiments at modest depths, are therefore complementary to most previous and existing cosmic ray muon studies which have been either much deeper underground or located on or very near the surface.

Indeed, unique data in a new muon energy domain can be obtained by equipping PA4 with arrays of muon chambers and scintillation counters. The importance of these studies follows from two considerations:

1. high-multiplicity muon events have not been studied with precise muon chambers over this range of muon energies (i.e. above 70 GeV, corresponding to a depth underground of 140 m) nor in conjunction with a surface air shower array; and
2. this is a particularly interesting energy regime from the point of view of the development of cosmic ray air showers, since it roughly corresponds to the characteristic energy at which the decay mean free path equals interaction mean free path for the pions produced in the original interaction.

1.2 Cosmic Ray Experiments with large underground detectors at CERN

It is important to note that the use of the large underground detectors at CERN for cosmic ray studies has previously been suggested by several groups, e.g. UA1 [11] and more recently by the LEP experiments. Members of the ALEPH collaboration started a pilot experiment (CosmoALEPH) by adding counter arrays underground around the ALEPH experiment over a distance of up to 1 km [12].

Since then the L3 experiment has established a cosmic ray experimental program, L3+Cosmics [13] which has taken data in parallel with the normal L3 readout. It has, as a principle aim, a precise measurement of the inclusive cosmic ray muon spectrum between 20 and 2000 GeV, in the context of the current interest in neutrino oscillations and the pressure for a more precise calculation of the muon-neutrino spectrum.

The utility of LEP experiments based data for cosmic ray studies has already been explored by the CosmoLep group in an analysis of multi-muon events recorded by the ALEPH experiment, using triggers during normal e^+e^- data taking [14]. In fact, the present proposal was motivated in part by the intriguing high multiplicity cosmic ray muon events observed with the ALEPH detector.

1.3 The cosmic ray spectrum

A primary cosmic ray nucleon will, on the average, have its first interaction with an air nucleus at about 20 km above the earth's surface, starting an electromagnetic and hadronic cascade which develops in the 1000g/cm^2 thick atmosphere. Photons, electrons and muons are the dominant particles that will reach the ground level; underground only muons will survive. The primary cosmic ray flux, as measured by a variety of experiments in recent decades, is shown in Fig. 1.1 [15]. At the lowest energies, where the rates are high, the most precise measurements have been made with balloon and satellite experiments using small (square meter or less area) detectors. These experiments can observe directly the primary interaction, and study the particle composition of the primary cosmic rays. As a result, the spectrum of cosmic rays at the top of the atmosphere has been well established over several orders of magnitude for energies below 10^{14} eV. For higher energies, the event rate becomes too small for balloon or most satellite experiments, and larger-area ground based experiments are required to study cosmic rays at high energies. It may be noted that an experiment, ACCESS, is being designed for the International Space Station for the specific purpose of studying the primary cosmic ray composition above 10^{14} eV by direct observation [16]. Interestingly, at energies between 10^{15} and 10^{16} eV, a very prominent and well-known feature of the cosmic ray spectrum appears; a break in the spectral slope which is known as the "knee" of the spectrum. Cosmic rays up to this energy range are thought to be of galactic origin, and hence the knee presumably represents some of the cosmic acceleration mechanisms reaching their maximum energy. This is also the energy range corresponding to the limit of confinement of the cosmic rays in the galactic magnetic field.

While the energy spectrum is reasonably well established, the composition of cosmic rays above energies of about 10^{14} eV is still unsolved and the subject of much active research. The present data on the particle composition of cosmic rays as a function of the incident energy is shown in Fig.1.2 [17], where the average of the logarithm of the mass number is plotted vs. energy, as deduced from a large number of experiments. At energies well below the knee, protons and light nuclei dominate. Around the knee there seems to be a transition to heavier nuclei, but the various experiments reach very different conclusions, and the situation is still unclear. Qualitatively, as heavier nuclei of the same total energy have a smaller radius of curvature in a given magnetic field than lighter nuclei, one expects that the galactic confinement would fail for protons and light nuclei at lower energies than for heavier nuclei, leading to a natural increase in $\langle \ln A \rangle$ with energy through this region.

Among the best recent measurements are results from the KASCADE experiment [7] in Karlsruhe, which consists of a surface array of electromagnetic and muon detectors deployed over an area of $200 \times 200 \text{ m}^2$. One of the basic difficulties in interpreting these data in terms of the mass and energy of a primary cosmic ray is the fluctuation in the shower development in the atmosphere, and in particular in the modelling of the forward particle production in the primary interaction. It is worth noting that results from HEGRA, MACRO, DICE and MSU would rather favour an almost energy-independent particle composition, in contradiction to the KASCADE measurements. Or could these discrepancies stem from the fact that the experiments measure in different kinematical regions, e.g. HEGRA in 2200m height and MACRO at about 1 km underground, corresponding to a 1.3 TeV muon cut-off?

1.4 Muons in air showers

Since the primary interaction occurs about 10 interaction- and 30 radiation- lengths above the earth's surface, measurements with large air shower arrays at ground level are only modestly sensitive to the characteristics of the first interaction. As a result, some observable quantities, like the electron and photon densities, are almost calorimetric in nature. As an example,

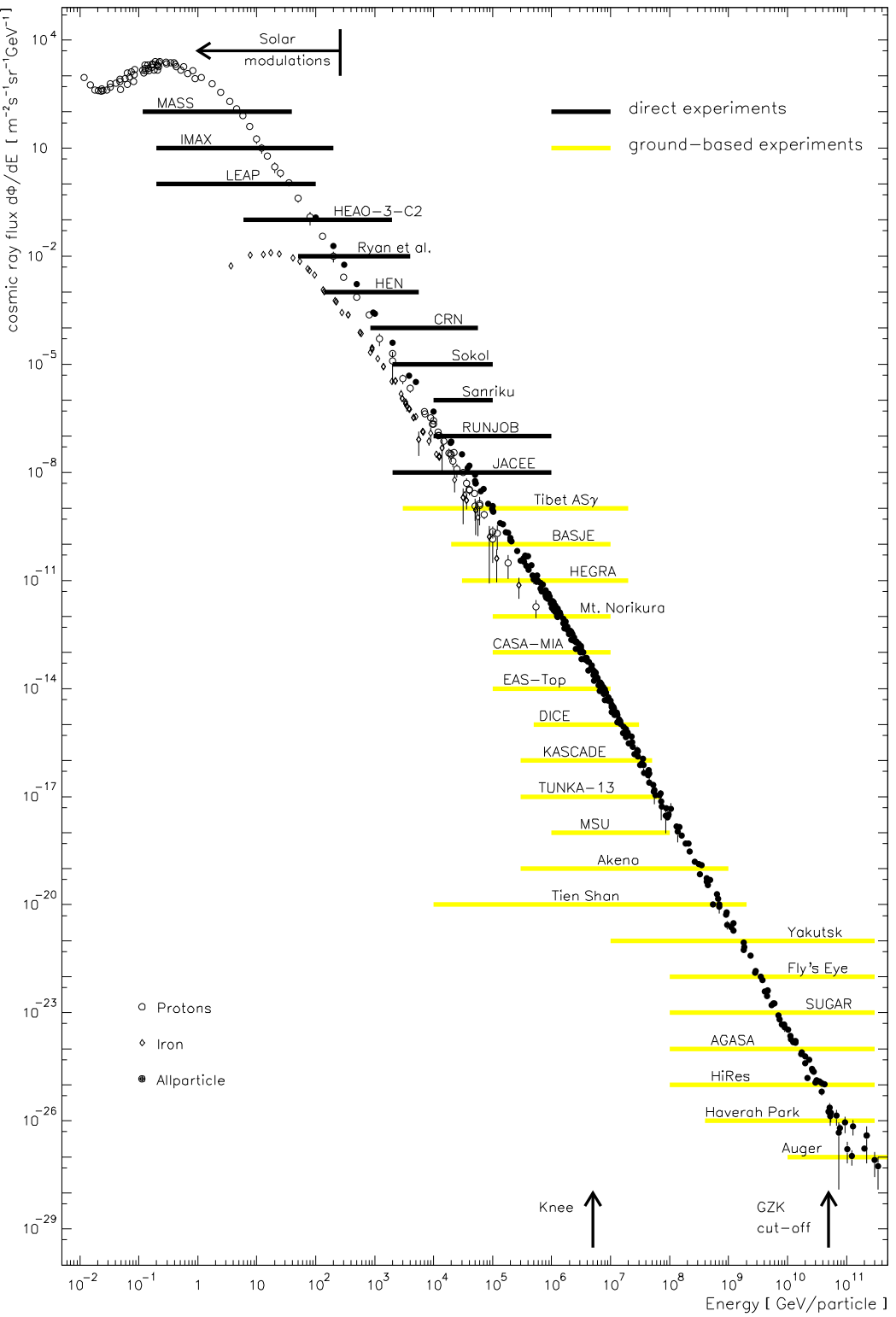


Figure 1.1. Energy spectrum of primary cosmic rays with the energy ranges of the experiments (taken from [15], where the indicated experiments are also referenced).

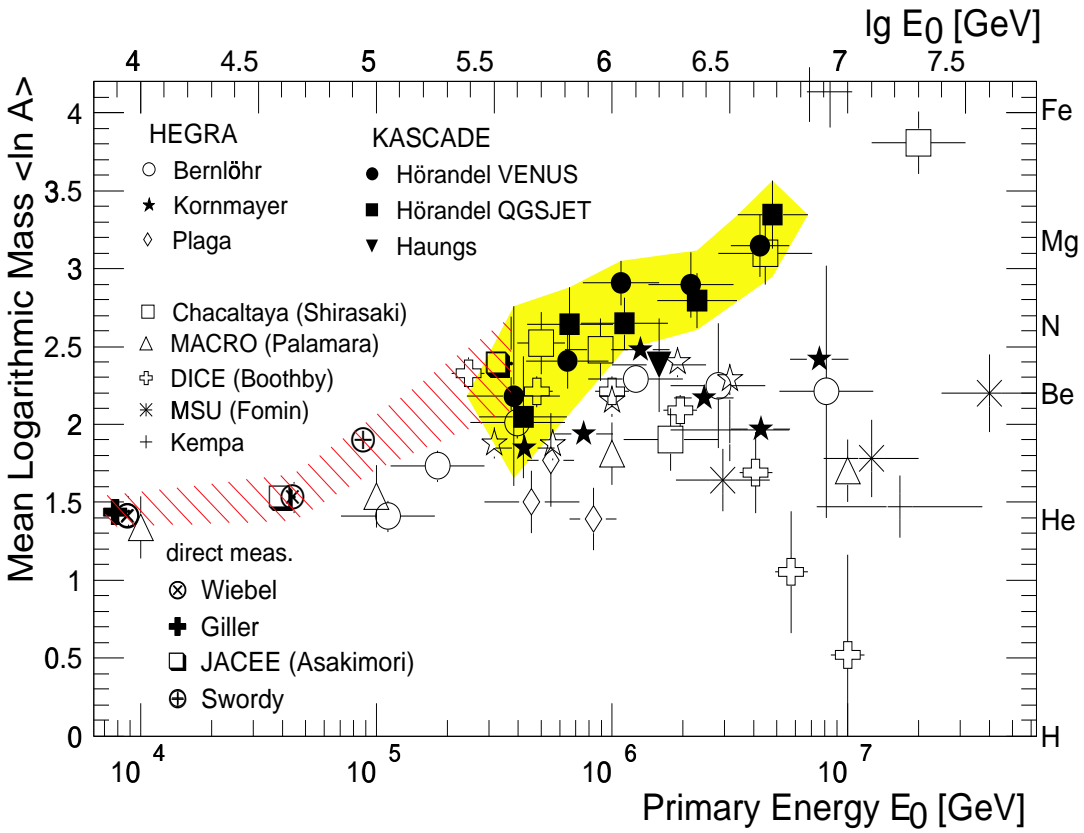


Figure 1.2. Chemical composition of primary cosmic rays (from [17]).

a shower area can be defined in which the integral number of charged particles is almost independent of the primary nuclei and only depending on the energy. This has been important in establishing the energy spectrum.

In order to efficiently trace back some details of the first interaction and to probe the primary cosmic ray composition, a maximum set of observables should be used. Muons, because they originate from the decay of pions and kaons and do not multiply but only lose energy by ionization as they traverse the atmosphere, are particularly useful in this regard. Hence muon data, detected with an experiment under a suitable overburden, are complimentary to experimental observations of cosmic ray air showers at ground level.

1.5 Underground muon experiments

Cosmic ray muon measurements, begun around 1937, are being continued in modern underground experiments, some of which were originally designed as proton lifetime experiments. The cosmic ray muon flux is steeply falling with energy (Fig. 1.3), hence with depth in the earth, or overburden, which may be expressed in m water equivalent (w.e.) or hg/cm^{-2} . The underground locations of several of the major experiments are indicated on the Fig. 1.3 by their overburden range over which they measure muons. Except for the underwater experiments, which have a rather crude spatial resolution, many of the experiments are deep underground, with a typical momentum cut-off of a TeV or greater. These experiments study the topological properties of multi-muon events for high-momentum muons. Due to the low rate, these detec-

tors are large and hence their granularity is modest. Other experiments, closer to the surface, usually have ionization detectors only and also lack precise tracking.

The size of the detector area, the spatial resolution, and the pattern recognition in complicated high-density events play a critical role in multi-muon studies. In this context, CORAL, with its location at about 300 m w.e. and under a geologically well known rock overburden, will provide unprecedented new data on the cosmic ray muon component of air showers. An additional virtue of CORAL is the near-by location of the Jura mountains; by choosing a zenith angle greater than 70 degrees and observing at a northwest azimuth, the overburden can be increased to more than 10 km w.e. This permits simultaneous measurements at very different overburdens.

The nearest analogue to CORAL would be the Baksan Underground Scintillation Telescope (BUST), at a depth of 850 m w.e. (energy threshold about 200 GeV). This 17x17 m² array of 0.7 x 0.7 x 0.3 m³ scintillators, arranged in four layers, also operate in conjunction with a surface “carpet” array. However, the tracking precision is limited by the scintillator sizes, and certainly does not approach either the precision or multiplicity resolution of the CORAL tracking chambers.

It is an advantage that different muon cut-off energies can be chosen by the amount of overburden in an underground experiment. Studies of very high energy muons in experiments deep underground probe different aspects of the shower than do the low-energy muons observed by surface experiments which come from the part of the longitudinal shower development where the pion density is largest. Conversely, muons with TeV momenta preferentially arise from decays at the top of the atmosphere. But they are also not ideal to characterize the primary interaction since due to the Lorentz factor only a small fraction of the hadrons will decay.

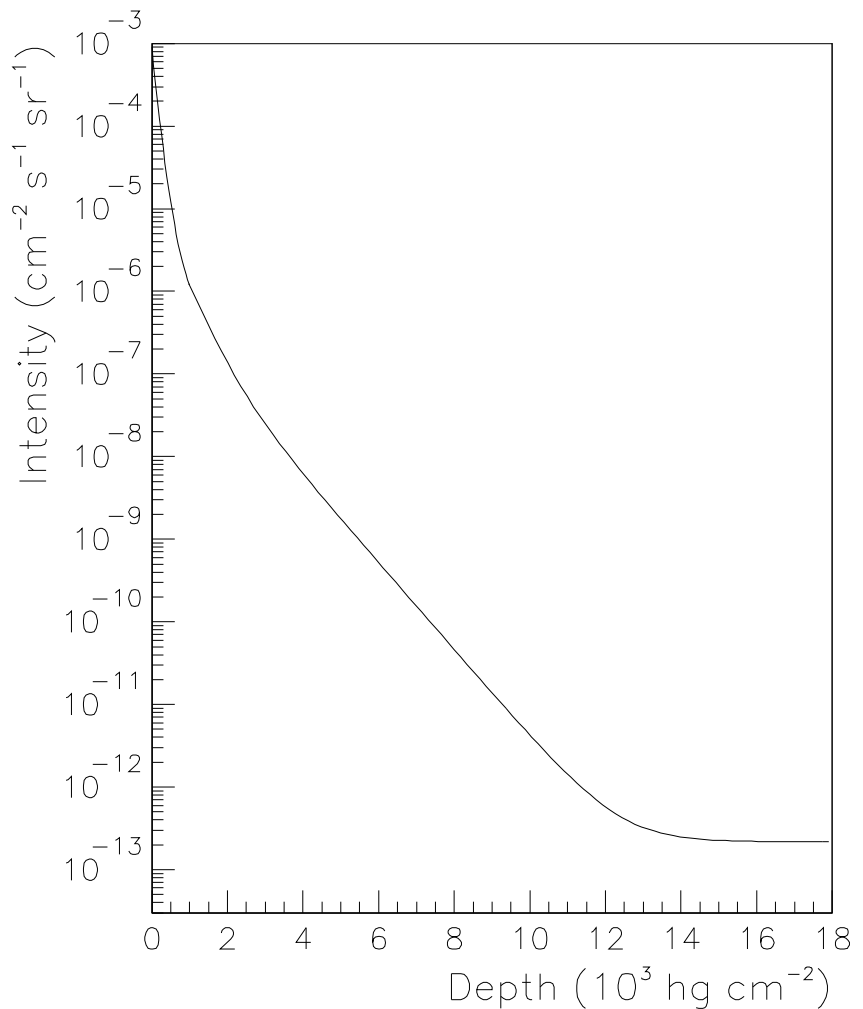
The optimal muon energy is around 50 - 100 GeV. At this energy the parent pions have a decay mean free path of about 5.5 km. At a height of about 15 km, corresponding to an atmospheric overburden of 120 g/cm², the decay mean free path and the interaction mean free path for the produced pions of the above energy are comparable and therefore a sizeable fraction of the muons are born at this height reflecting some properties of the primary interaction.

It is a unique feature of the CORAL experiment that it operates in the vicinity of this “characteristic energy” of about 100 GeV.

1.6 Cosmic Ray Results Obtained with the ALEPH Detector

The present proposal was motivated in part by the intriguing high multiplicity muon events observed in an initial experiment with the ALEPH detector. The contributions of this experiment to the study of multi-muon bundles from cosmic rays result from the superb characteristics of the ALEPH detector [18] which was located at the deepest LEP point, 140 m underground, corresponding to a momentum cut-off of 70 GeV for vertical muon incidence. The large Time-Projection-Chamber (TPC) inside a solenoidal field of 1.5 Tesla provides excellent pattern recognition, tracking resolution and momentum determination. The TPC was surrounded by electromagnetic and hadronic calorimeters with tracking capabilities and by an outer shell of muon chambers.

Standard LEP triggers of ALEPH were also sensitive to cosmic ray muons, particularly multi-muon events, if they occurred within a gate of a few microseconds centered on the electron-positron beam-crossing times. The cosmic events were triggered by the energy deposition of the muons in the electromagnetic and hadronic calorimeters. About 580 000 cosmic ray events were selected from the LEP data taking periods during the years 1997 to 1999, corresponding to an effective data taking time of $1.7 \cdot 10^6$ sec. A representative sub-sample of the data was scanned, as were all events with multiplicity greater than 6, in order to remove beam-gas and muon interactions that can simulate high-multiplicity events.



CosmoLep, 24x14 m ²	_____
underwater exp.	_____
MACRO, 12x76 m ²	_____
SOUDAN, 8x16 m ²	_____
SCE/NUSEX (Mt. Blanc), 8x7 m ²	_____
Kolar Gold Fields, 6x16 m ²	_____
BAKSAN, 17x17 m ²	_____
LVD, 40x13 m ²	_____
Fréjus, 6x12.3 m ²	_____

Figure 1.3. The muon flux as a function of depth as measured by underground experiments [19]. The depth ranges of some experiments are also drawn. References: underwater experiments – see [19]; MACRO – [2]; SOUDAN – [20, 21]; SCE – [22]; NUSEX – [23]; Kolar gold fields – [24]; BAKSAN – [25, 26]; LVD – [27]; Fréjus – [5, 6]

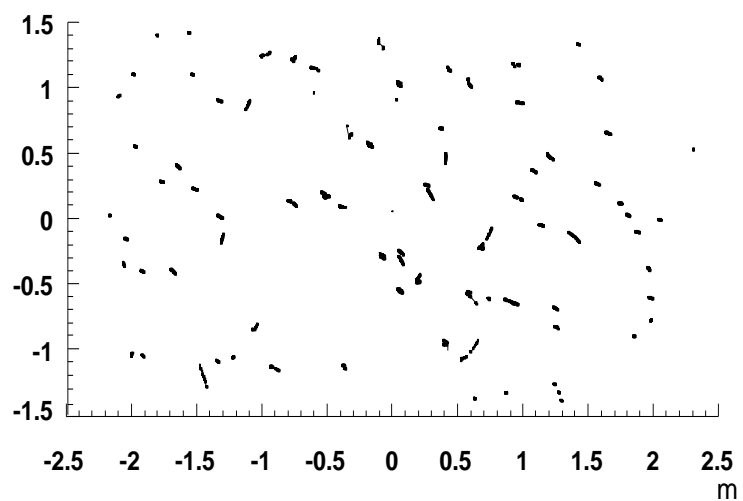
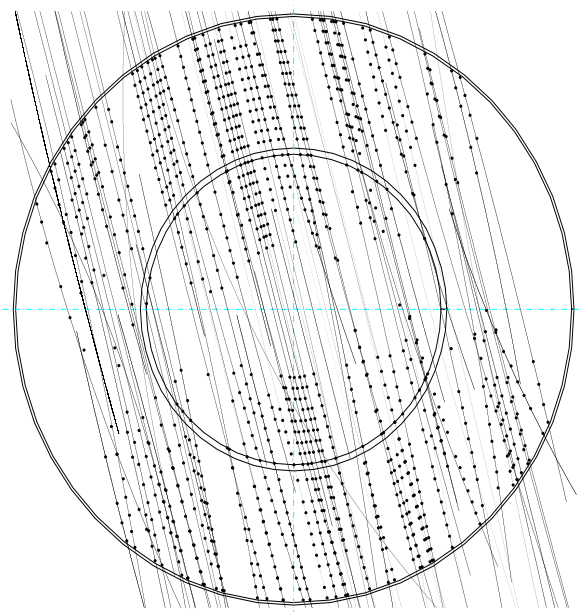
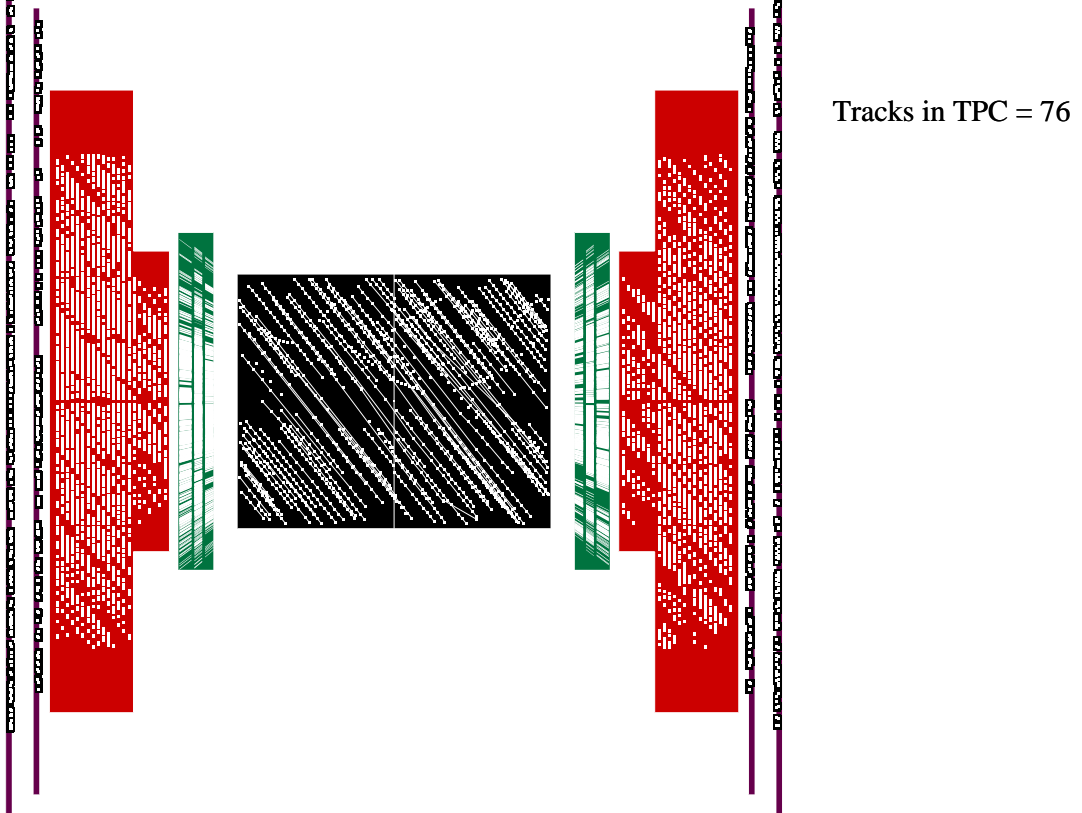


Figure 1.4. A high multiplicity event (76 tracks) in three different views: perpendicular and along the LEP ring and along the muon shower direction.

As an example, one of the highest multiplicity muon events is displayed in Fig. 1.4 with views along and perpendicular to the LEP ring and also perpendicular to the muon shower direction. The excellent resolution of the TPC easily resolves close-by muon tracks and enables an angular determination to better than 5 mrad, the average multiple scattering angle of the muons in the 140m overburden. Further information about the muon density is given by the forward calorimeters and muon chambers. The 76 recorded tracks in the TPC appear as points in the plane perpendicular to the muon bundle axis for those muons which are parallel to the shower axis. As seen in Fig. 1.4, the muons are almost parallel and are distributed isotropically over an area of $4 \times 3 \text{ m}^2$. The large muon density of about 6 muons/m^2 extends further into the forward calorimeters.

For quantitative analysis, the ALEPH data were compared with the expectations from cosmic ray air shower simulations (see Section 4 for details of the CORSIKA shower simulation). Fig. 1.5 shows the measured distribution of the muon multiplicity in the TPC and the QGSJET CORSIKA simulation for proton and iron primary particles, absolutely normalized to the effective running time. Up to a multiplicity of 20, the proton curve describes the observed data well over several orders of magnitude, indicating that the primary spectrum is dominated by light elements at energies corresponding to these multiplicities. The discrepancy in the single muon rate is due to the low efficiency of the LEP triggers for single muons; this efficiency approaches 100% only if there are more than two muons in the TPC. At larger multiplicities there is evidence for a transition to the iron curve. Iron induced showers are more effective in producing muons (see Fig. 1.6) since they interact higher in the atmosphere and also produce larger pion multiplicities. While the simulation agrees with the data over a wide multiplicity range, it fails to describe the highest multiplicities, even under the assumption of a pure iron composition. Tab. 1.1 summarizes the characteristics of the five highest multiplicity events. An estimate of the primary energy was made under the assumption that the shower center is in the TPC and taking into account the zenith angle. The energy was calculated assuming proton-induced showers and would be 40% lower for iron. If the shower cores were further away, the energies would be even larger.

It should also be mentioned that anomalous high multiplicity muon events have also been reported by the BUST [28] and Kolar Gold Fields [29] experiments.

event	muon density (m^{-2})	zenith angle ($^\circ$)	primary energy (eV)
97-a	4.75	40.8	$3 \cdot 10^{16}$
97-b	5.3	37.7	$3 \cdot 10^{16}$
97-c	8.9	40	$6 \cdot 10^{16}$
98-a	8.2	48.6	$7 \cdot 10^{16}$
98-b	18.6	27	10^{17}

Table 1.1. Characteristics of the highest multiplicity events. The primary energy was estimated by assuming the shower center to be close to the TPC and taking into account the zenith angle.

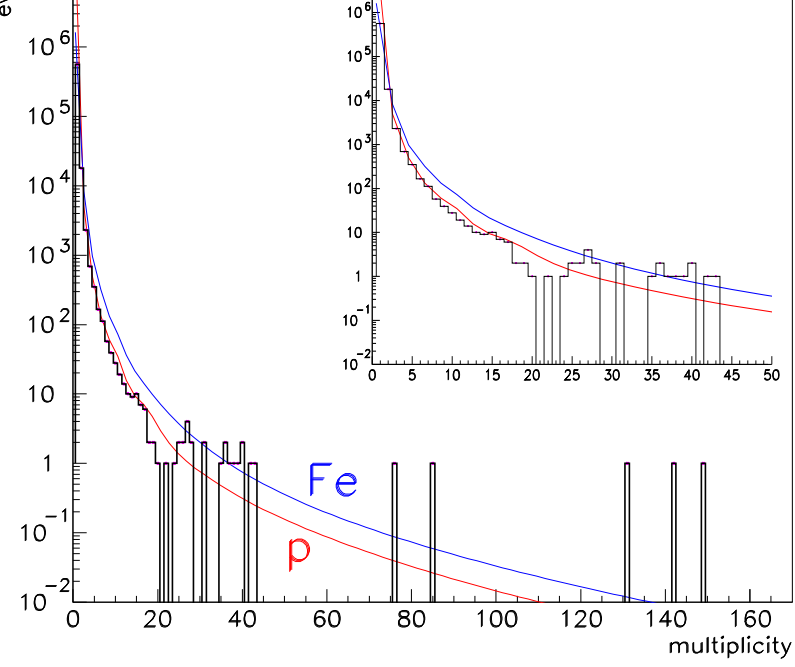


Figure 1.5. Multiplicity distribution of muons in the TPC compared to CORSIKA simulations for p and Fe as primary particle. The highest multiplicity event has twice the particle density (see Tab 1.1)

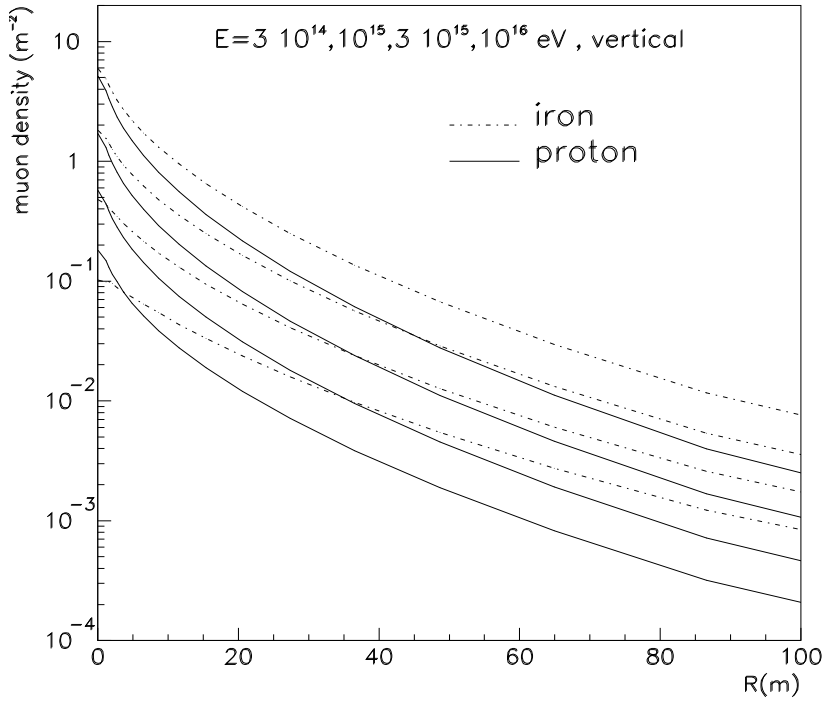


Figure 1.6. CORSIKA Monte-Carlo simulations of the muon density for proton and iron induced showers of various energies as a function of the radial distance from the shower center

1.7 Capabilities of the CORAL Detector

As noted above, the ability to resolve close-by muons in even dense muon bundles and to measure the muon density and its spatial extent over a sizeable area (400 m^2) will be a powerful tool to reconstruct the primary energy and composition. The transverse size of muon bundles is sensitive to the mass of the primary nucleus. Fig. 1.6 illustrates the radial muon distributions produced by proton- and iron-induced air showers for three different energy ranges, as calculated with CORSIKA simulations (see Section 4). Three distinct features of the radial distributions are relevant to our studies: the muon density in the center is almost independent of the primary nuclei mass and increases linearly with the primary particle energy. This allows an energy determination, independent of the primary particle mass. The density decreases by an order-of-magnitude over a distance of some 10 m from the core center. Compared to the extension of an air shower in the top array the muons with a momentum cut-off of 70 GeV are concentrated over a much smaller area. Hence the underground muon area of the CORAL lay-out is well matched in investigating most of the muon bundles, initiated by primary cosmic rays in the energy range of $10^{15} - 10^{17}$ eV.

Compared to protons, iron induced muon bundles exhibit a flatter radial distribution and contain twice as many muons. This is due to the characteristics of iron-air interactions which start higher in the atmosphere and produce more pions.

In principle, a precise measurement of these muon bundles would be sufficient to determine the primary energy and the composition if the interaction characteristics would be precisely known. But in combination with an independent determination of the shower characteristics at the ground level, the identification of the primaries is drastically improved.

The ability of the CORAL detector to distinguish between different species of cosmic ray primaries by combining information from the underground muon array with information from the surface air shower array is indicated in Fig. 1.7.

By using these techniques, CORAL will determine the primary particle species with an unprecedented precision for primary energies from 10^{14} eV to a few times 10^{16} eV.

1.8 Other Possible Surprises

At the knee, the primary collision of a cosmic ray with the nuclei in the atmosphere corresponds to a center-of-mass energy somewhat above that probed in $p - \bar{p}$ collisions at the Tevatron. The Tevatron's 2 TeV c.m. energy is that produced by the interaction of a proton of 2×10^{15} eV with a stationary proton. Even at Tevatron energies many aspects of particle production are unexplored; little is known about the production of particles with less than the generic p_t of a few hundred MeV/c, i.e. the particles produced at small angles or high values of pseudo-rapidity η . There are ample reasons to expect surprises in this regime of energy and parameter space, which has been unexplored at particle accelerators. The uncertainties are even larger in the case of nucleon-nucleus and nucleus-nucleus collisions. One possible indication of such surprises has been provided by the JACEE Collaboration, using a balloon-borne emulsion chamber designed to probe the primary cosmic ray composition. They have reported several events exhibiting "Centauro" and "anti-Centauro" behaviour, an anomalously large or small ratio of photons to charged particles in a limited region of pseudorapidity-azimuth phase space. This could possibly be indicative of "Disoriented Chiral Condensate" (DCC) - like low p_t production [30]. One such event is illustrated in Fig. 1.8 [31].

The topology of these events can easily be recognized by the CORAL experiment. In one case, a large electromagnetic shower would be measured in the top array with almost no muon content underground, in the other case too many muons would be detected without the correspondent electromagnetic air shower. This is an example how the top and the underground

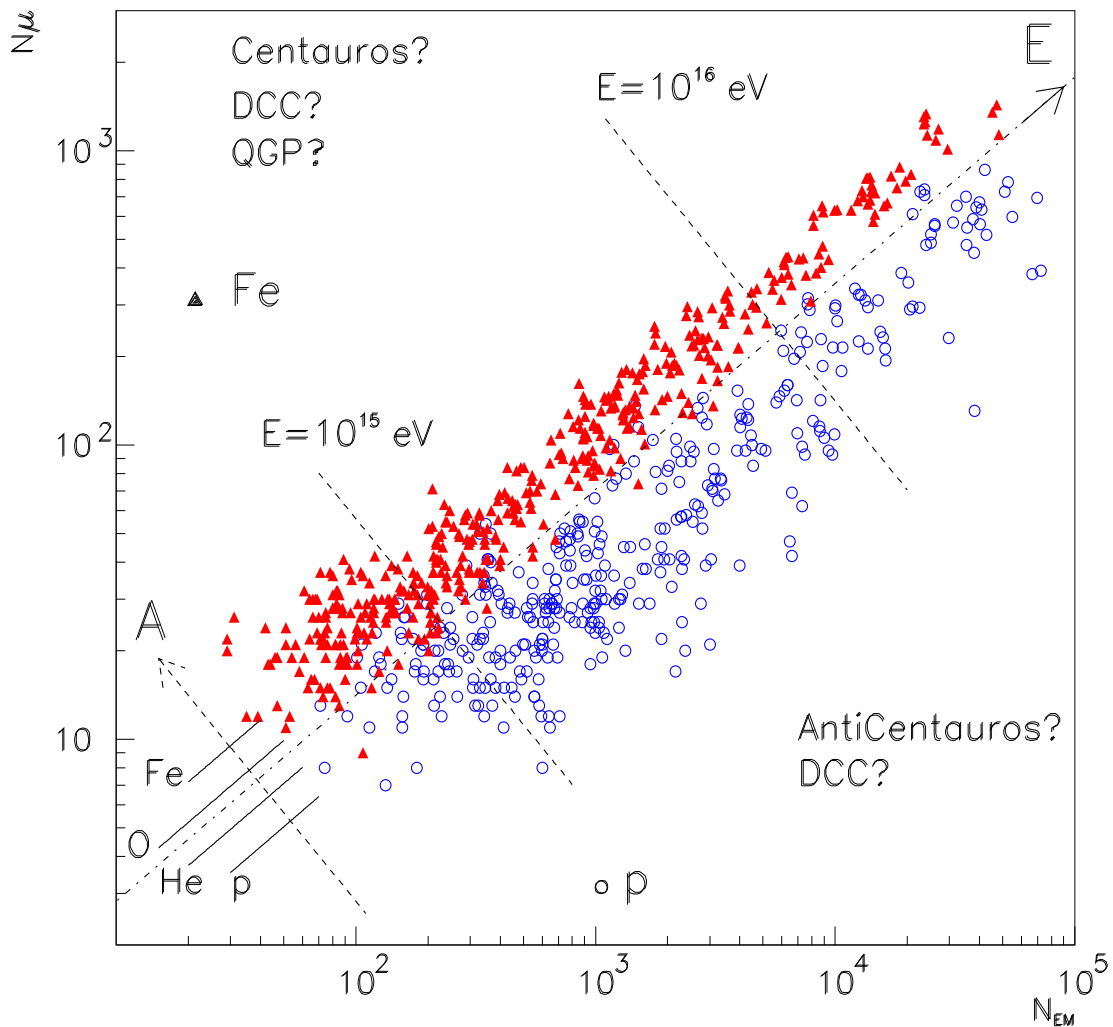


Figure 1.7. Number of muons ($p > 70 \text{ GeV}$) versus number of electromagnetic particle in an area of $100 \times 100 \text{ m}^2$, for proton and iron initiated showers, pointing to the center of the underground array within 10 m ($5 \cdot 10^{15} < E < 5 \cdot 10^{16}$, zenith angle $\theta < 15^\circ$). The primaries ($p, \text{He}, \text{O}, \text{Fe}$) cluster around the straight lines indicated in the plot.)

measurements help each other in interpreting the events.

The formation of a quark-gluon-plasma (QGP), e.g. in iron-air collisions at the highest energies, would also manifest itself in an outstanding large muon content. [32]

Another kind of surprise could be provided by stable bodies of strange quark matter. If present in cosmic rays, such bodies would break into hadrons through interactions with ordinary matter, giving rise to very narrow but slowly diverging beams of a large number of ultra-high energy particles. Such bodies would thus manifest themselves as a large number of small showers incident over a large area, quite distinct in properties and structure from the usual cosmic ray showers. Such groups of showers can be searched for by looking for correlations among surface air shower arrays separated by distances of at least a few kilometers. CORAL will search for such events in cooperation with the 50-detector L3C array operational above the former L3 experiment. Correlating with other local stations would enhance the statistics and enlarge the detection area.

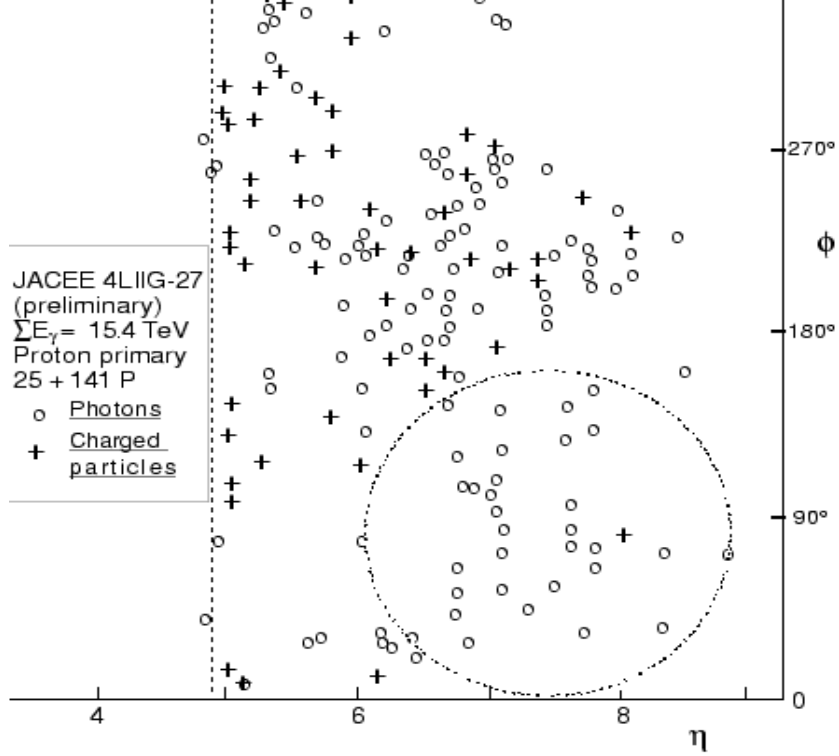


Figure 1.8. Example of a high multiplicity event with an anomalous concentration of photons in a limited range of phase space [31].

1.9 Muon Astronomy

With its precise measurement of the muon direction, 10 mrad for a single muon and statistically better for multi-muons, the CORAL detector can also be used as a telescope to seek point sources in our galaxy and possibly beyond [33]. But for energies of charged particles well above EeV, for which the trajectories are not scrambled by galactic magnetic fields, the data rate for CORAL is too small to be of use.

Consequently, muon ‘astronomy’ can only be performed with neutral primaries such as photons, neutrinos, neutrons, or exotic particles (SUSY particles, “strangelets”, dust grains, etc.). Such neutral parent particles, which carry the directional information, may undergo an interaction in the atmosphere producing muons, which would then be detected by CORAL.

Photons with energies in excess of 300 TeV are absorbed by the blackbody microwave photons, thus reducing their mean free path to about 10 kpc. For photons with energies above 10^5 TeV, the cosmos again becomes more transparent. Although less efficient than hadrons in producing muons, photon-initiated showers would produce muons via pair production and through photo-production of hadrons from air nuclei.

Muon neutrinos, detected via charge exchange, would also point to their source, but, due to background from atmospheric cosmic rays, only upward-going muons would be useful, and the rates would certainly be low.

Very energetic neutrons may be produced through protons or nuclei interacting with the plasma environment in an accelerating shock; from 300 GeV experiments, the cross section for producing neutrons of nearly the full proton energy in inelastic collisions is quite high. However the neutron lifetime constrains the range of ‘neutron astronomy’ to our local galactic neighbourhood; the decay path-length is about 100 pc at 10 PeV. To be sure, at energies approaching an

EeV, neutrons could permit us to scan most of our galaxy for sources, flux permitting.

Exotic particles (e.g. WIMPs) may exist, but their interaction cross-sections are small and the chance to find them with CORAL would appear to be small. Strangelets (nucleus-like stable neutral objects containing equal numbers of up, down, and strange quarks) have been postulated, and, if of energies of a PeV or greater, would initiate air showers in line with their origin. At this time, their stability is uncertain and they remain undetected. Dust grains, originally charged during acceleration and then neutralized, might be candidate neutral particles, but almost certainly not of sufficient Lorentz factor to generate air showers.

These arguments suggest that the most promising point-source candidates for muon production may be photons. There are known sources of TeV gamma-rays in our galaxy as well as at extra-galactic distances. Atmospheric Cherenkov observations have confirmed that familiar sources as well as those discovered by the Compton Gamma Ray Observatory (CGRO) in the GeV range extend into the TeV range, and even beyond [34]. The most promising sources are the Crab nebula, the pulsar PSR 1706-44, and the active galaxy, Markarian 421. The gamma-ray spectrum of the Crab nebula, for example, is known to extend beyond 10 TeV [35, 36]. Sources such as Markarian 501, which emit photons above the TeV range, are not seen by detectors such as the CGRO.

Earlier there had been claims of observations of astronomical sources from air showers and from muon detectors [38, 39], but more recent, intensive sky searches, by the MIA-CASA array for example, have failed to confirm the earlier sightings [9]. The negative results from CASA-MIA [34], and from other searches within the past decade, suggest that such sources, if they exist at energies above 10^{14} eV, are faint and/or variable. To be sure, it would not be unreasonable that such sources would be variable and, perhaps, sporadic. So there is indeed room for surprises.

Muons from such sources must compete with a large background of muons from charged primary cosmic ray induced atmospheric air showers; a charged primary is about two orders of magnitude more efficient in producing muons than a primary gamma of the same energy. Therefore, point-source muons can only be identified if the collecting power and angular resolution of the detector are very good. The sources may be highly variable, possibly producing a significant signal over a short time only.

The signature in CORAL will be single-muon or multi-muon events together with a photon shower on the top. For the signal to stand out from a background uniformly distributed in space and time, a good angular resolution of the muon detection is required. The tracking system of the CORAL detectors will provide an excellent angular resolution of a few millirad. Due to multiple scattering in the 140 m of molasse rock overburden, the pointing accuracy will be limited to about 10 mrad (for muons of about 100 GeV). For multimuon events, the angular accuracy will be somewhat better. The effect of the Earth's magnetic field on the deflection of positive and negative muons is also on the order of 10 mrad or less, depending on the muon energy.

2 Results from the test set-up in the underground area at BA4

The large multiplicity events in ALEPH were observed with a Time-Projection-Chamber (TPC), one of the best tracking devices used in particle physics. The principal thrust of the CORAL proposal is to extend these measurements by installing a large array of muon tracking chambers in order to increase the statistics and to study the radial structure of multimuon events over a large area.

The muon detectors from the UA1 and the DELPHI experiments are well suited for the underground array. Both detectors are robust multi-layer drift chambers with ± 7.5 cm (UA1, [40]) and ± 10 cm (DELPHI, [41]) drift space.

2.1 Performance of UA1 and DELPHI Chambers

In order to demonstrate that these chambers have sufficient resolution and two particle separation for the study of high multiplicity events, we installed a small test setup in the former UA2 underground area (BA4). Situated under some 50 m of overburden, the test setup provided important information about the operation of the chambers and the optimization of the final detector layout.

The following issues were addressed:

- The chambers were operated using a flammable gas mixture in previous experiments. This is now prohibited in underground areas. Can the chambers be operated on a non-flammable mixture without losses in efficiency or resolution?
- What is the maximum muon density which can be reconstructed in the chambers and how many layers of chambers are needed?
- Is an absorber between the chambers useful in distinguishing muon bundles from muon induced showers in the rock?

Fig. 2.1 shows a photograph of the actual test set-up in the UA2 area. Four UA1 muon chambers ($4 \text{ m} \times 6 \text{ m}$) are placed on top of each other with a precision of better than 0.5 mm via spacers linked to four precise fiducial plates. These chambers are composed of individual extruded aluminium tubes which are glued together to form a rigid and self-supporting chamber body of four layers, two per projection. Two adjacent planes of staggered tubes help to solve the left-right ambiguity inherent in drift chambers and to overcome the inefficiency due to the gap between the tubes.

Two double-plane DELPHI chambers were mounted on top of the UA1 chambers. One coordinate is given by the drift time, the other, along the wire, by the longitudinal readout via a delay line.

The array was triggered by counters placed between the chambers. A 10 cm iron absorber was mounted between the two top and the two bottom UA1 chambers during a portion of the run. The drift time was recorded with 1 nsec precise drift time digitizers which had a multiple hit capability of 16 hits per wire. The data contained single and multi-muon events with up to 100 muons per event, as well as muon induced showers.

We investigated the properties of the chambers for several non-flammable gas mixtures. Mixtures containing only Argon and CO_2 were not optimal. Either the efficiency plateau was too short (95 % Ar / 5 % CO_2) or the drift time - distance conversion was nonlinear (80 % Ar / 20 % CO_2). Satisfactory results have been obtained by a further addition of CH_4 . We have chosen 90 % Ar/5 % CO_2 / 5% CH_4 as an optimum mixture. For this gas mixture, the efficiency plateau is given in Fig. 2.2-a and the efficiency dependence on the drift distance in Fig. 2.2-b. The hit residuals as a function of drift time are shown in Fig. 2.2-c. The final hit resolution of the UA1 chambers after calibration are shown in Fig. 2.2-d.



Figure 2.1. The actual test setup in the UA2 area.

The corresponding graphs for the DELPHI chambers are shown in Fig. 2.3, together with the additional residual distribution along the wire from the delay line. The spatial resolutions of the UA1 and the DELPHI chambers are summarized in Tab. 2.1. While we mainly took single muon

Detector	UA-1 chambers		DELPHI chambers	
Condition	$ \alpha < 15^\circ$	$15^\circ < \alpha < 30^\circ$	anodes	delay lines
RMS of residual distribution	0.81 mm	0.84 mm	0.79 mm	8.4 mm

Table 2.1. Drift chamber coordinate resolution (α is a track angle with respect to the vertical direction).

data at the beginning in order to find the optimal running conditions for the chambers, a multi-muon trigger was installed during the final months. About $2.4 \cdot 10^6$ events were recorded with this trigger during an effective running time of about $3.7 \cdot 10^6$ sec. In addition to multi-muon events, the data also contained muon induced showers which can simulate high-multiplicity muon events. However, these events could easily be eliminated during the scanning due to their different topology. In contrast to the multi-muon events in which the hits are almost isotropically distributed over the entire chamber, the showers are more concentrated over a smaller area. Fig. 2.4 illustrates the hit topology of a multi-muon event; this should be compared to the shower event of Fig. 2.5. Unambiguous and event topology independent criteria can be applied if the top and the bottom chambers are decoupled by an absorber. For this study, a 10 cm thick iron absorber was installed. For muon induced electro-magnetic showers the absorber reduced the hit density by a factor 3 on average, leaving the hit density for multi-muons uninfluenced. New

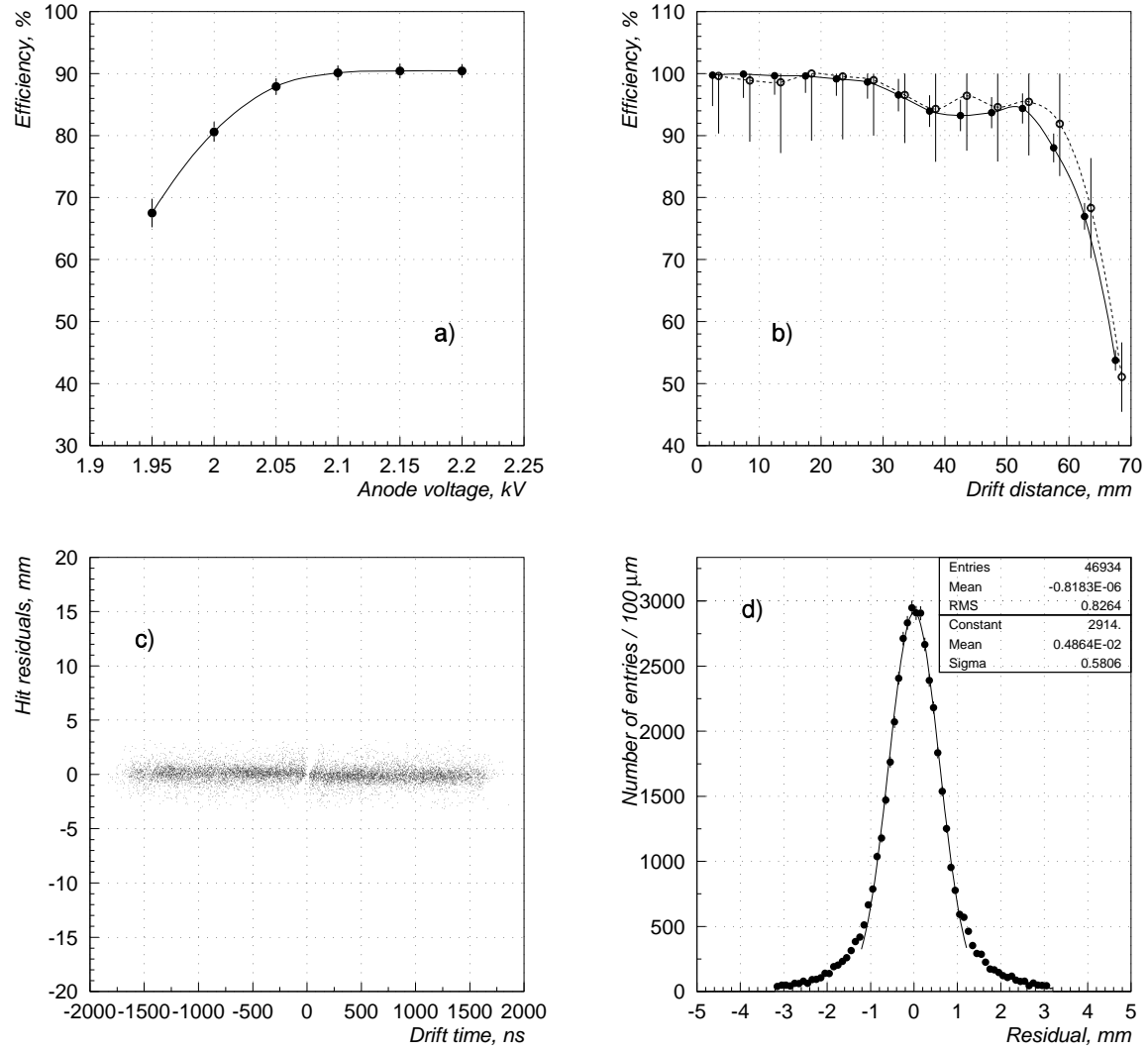


Figure 2.2. Calibration of UA1 chambers: a) drift chamber efficiency as a function of anode voltage for the Ar:CO₂:CH₄ 90:5:5 gas mixture; b) drift chamber efficiency as a function of the drift distance for the same gas mixture and anode voltage 2.1 kV. Full circles for track incident angles $-15^\circ < \alpha < 15^\circ$, open circles for $15^\circ < |\alpha| < 30^\circ$. Lines are drawn to guide the eye; c) hit residuals vs signed drift time; d) hit residual distribution.

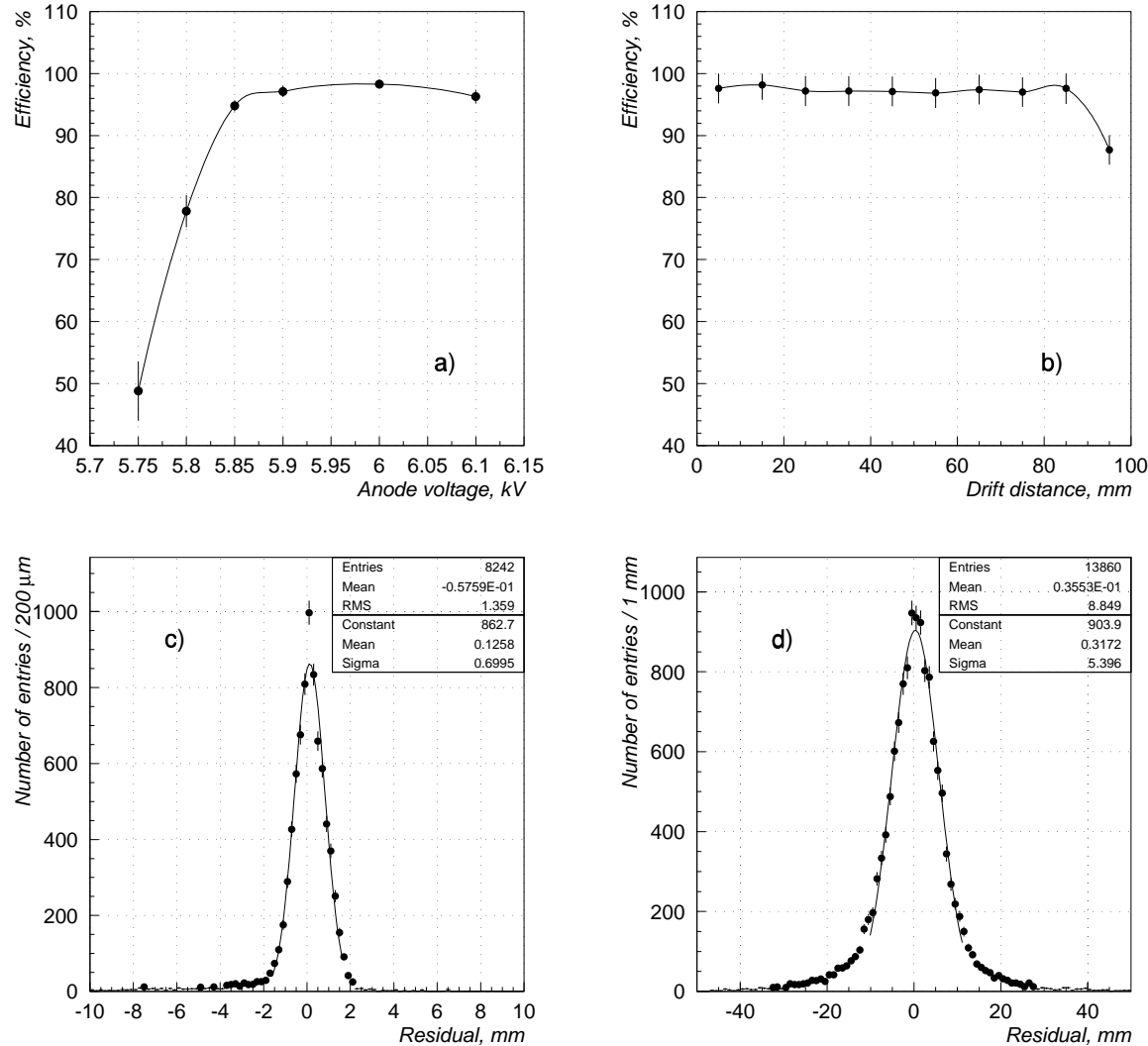


Figure 2.3. Calibration of DELPHI chambers: a) drift chamber efficiency as a function of anode voltage for the Ar:CO₂:CH₄ 90:5:5 gas mixture; b) drift chamber efficiency as a function of the drift distance for the same gas mixture and anode voltage 6.0 kV. Lines are drawn to guide the eye; c) hit residual distribution along the drift direction; d) hit residual distribution for the longitudinal read-out with delay lines.

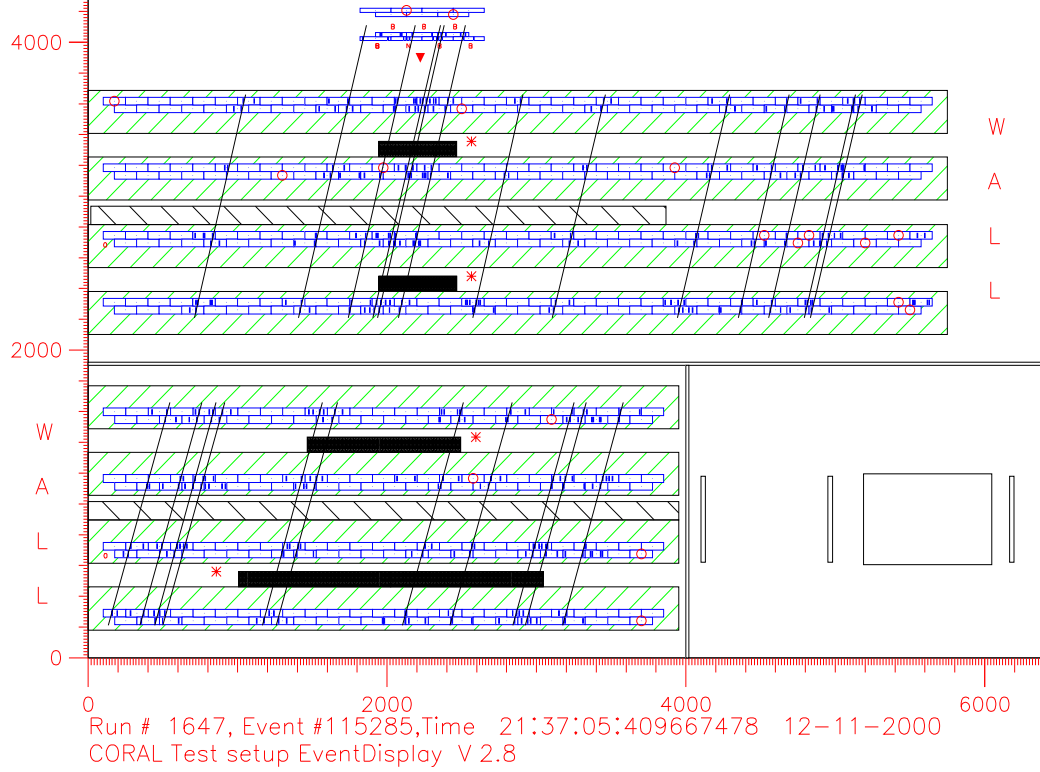


Figure 2.4. A multimuon event as displayed in two projections of the 6 m x 4 m muon chambers.

showers are created by muon interactions in the absorber with a probability of 1%; they have however, have a very limited extension over the chamber (see Fig. 2.6). The above experimental results were confirmed by detailed GEANT simulations. Muon induced showers can thus be identified by comparing the hit density above and below the absorber. As a consequence, a 50 cm thick absorber with a density of 4 g/cm³ will be placed in the CORAL experimental setup between the UA1 and the DELPHI chambers.

2.2 Reconstruction of multi-muon events

Tracking in very high multiplicity events is, in general, a challenge. The task is made much easier in CORAL because the tracks of interest, arising from multi-muon bundles, will be parallel to a rather high precision. Further, drift chambers will cover a significant area in the proposed experimental setup. As a result, it will be possible to start track finding in regions of lower occupancy. This will provide information about the direction of the muon bundle, which can then be used to define "roads" in higher occupancy regions of the detector.

The test setup in BA4 was of significantly smaller area, and muon bundles typically covered the entire detector area. In addition, the test stand at BA4 is at a depth of only 50 m overburden, as compared to the 130 m overburden present at PA4, where the CORAL experiment will be located. As a result, much lower energy muons ($p > 20$ GeV) make it to the apparatus, and hence the density of tracks per event is much higher than it will be the case in the final CORAL setup. Finally, the results reported here use only the four UA1 chambers mounted on top of each other, thus providing far less information per track than will be available with the final CORAL experimental setup. As a result, tracking in the test setup is a significantly more difficult proposition than will be the case with the final CORAL experiment setup.

In order to meet these challenges, a more global search algorithm has been developed based on a Kalman filtering approach [43]. All possible track candidates within $\pm 50^\circ$ of the verti-

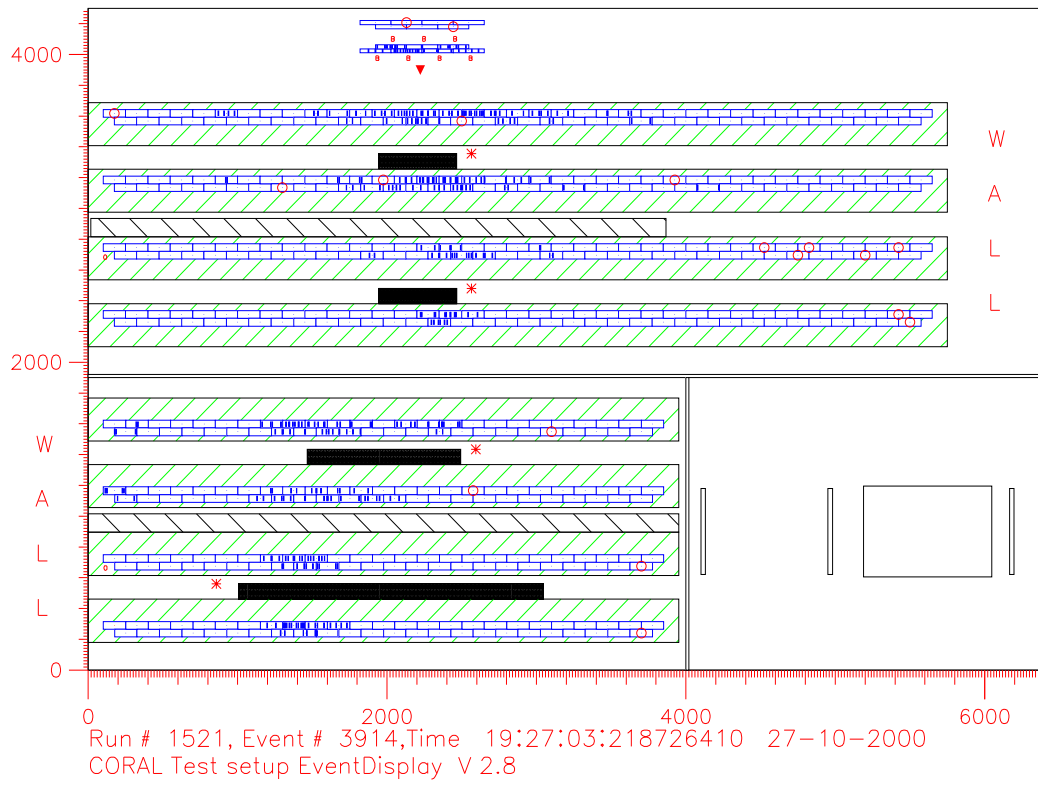


Figure 2.5. Shower from the rock of the overburden.

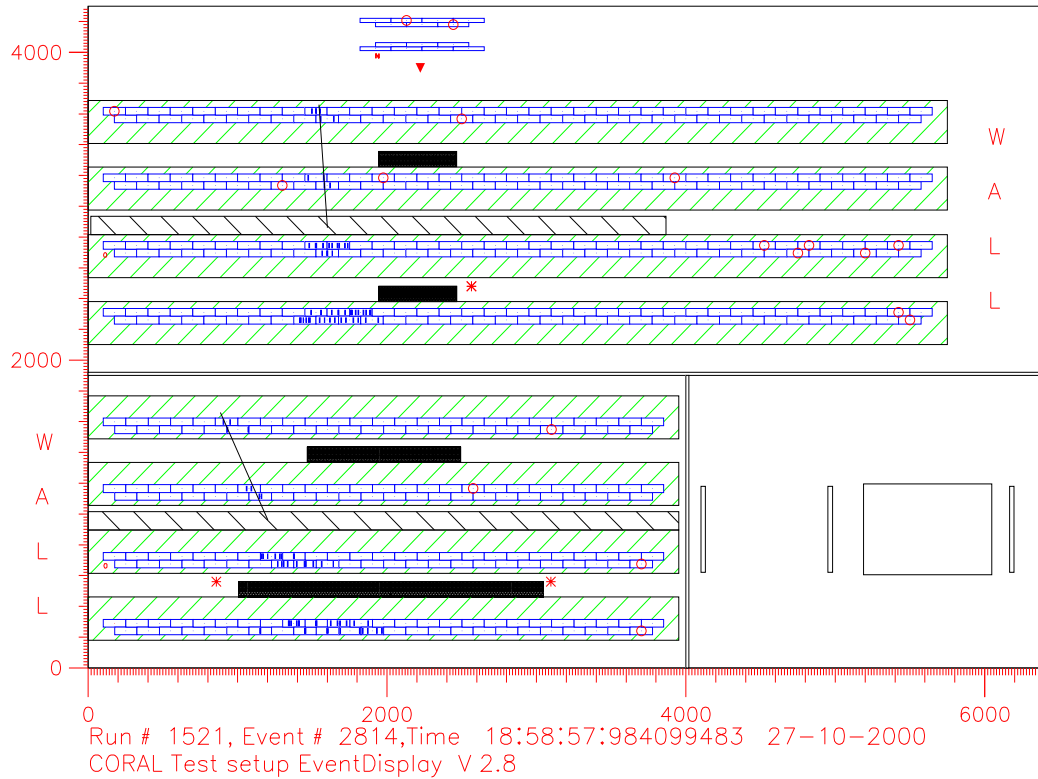


Figure 2.6. Muon-induced shower in the absorber

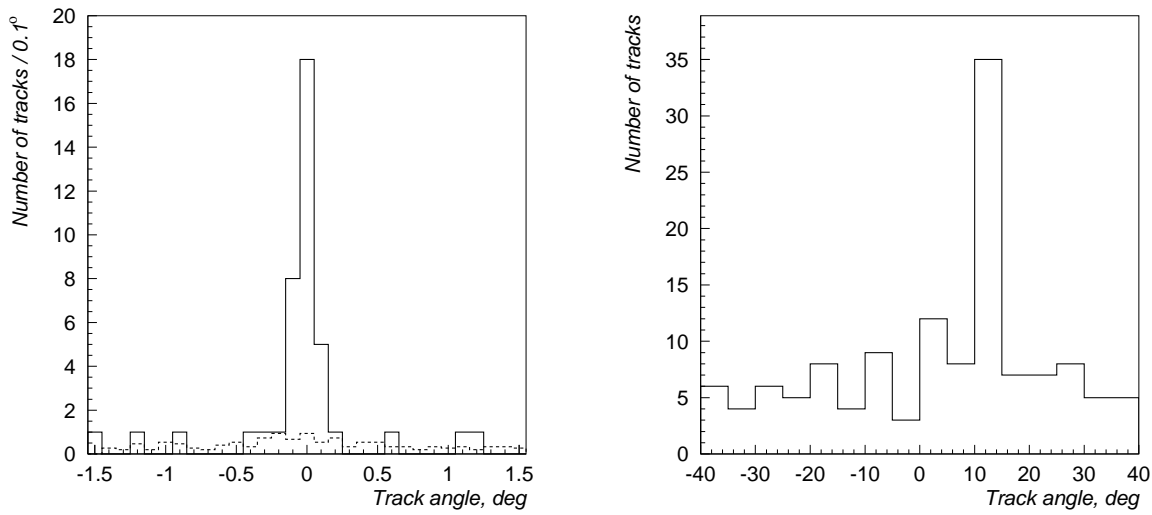


Figure 2.7. Left: distribution of angles of reconstructed tracks centered at zero for an event with a muon multiplicities of ~ 35 . Solid line - correct angle, dashed line - average of several wrong angles. Right: track multiplicity vs angle after an angular cut of $\pm 0.5^\circ$

cal are formed using any two hits from different planes. Track candidates are then propagated through the other planes, and hits are rejected if $\chi^2 > 10$ assuming a measurement error of 1 mm. Candidate tracks are accepted if they have at least 5 hits out of a possible 8, and at least one hit in each chamber. This yields a tracking efficiency of $\sim 95\%$ for a chamber efficiency of 90%.

After all track candidates have been found, they are used to find the most probable direction for the bundle. A track quality factor is then computed based on the number of hits in the track candidate, the χ^2 of the track fit, and its deviation from the most probable direction. The track candidates are then sorted according to quality, the best track is accepted, and its hits are subtracted from those of the other candidates. The quality of the other track candidates are then recomputed, and the procedure is repeated until all track candidates have been examined. The accepted tracks are used to refine the estimate of the probable direction of the bundle, and the procedure is repeated, with an additional requirement that the candidates be within 0.5° of the most probable direction. This cut removes a significant fraction of false tracks, as indicated in Fig. 2.7; the ability to find the angle is also illustrated in the same figure, where track multiplicities are shown for different angles.

Limited double hit resolution can also decrease tracking efficiency, particularly in high multiplicity events. This can be studied by altering the measurement error assumed in the tracking code, and can be addressed to some extent by judicious relaxation of track acceptance criteria. In particular, after the first iteration the acceptance criteria were relaxed by allowing some missing chambers, and then repeating the tracking algorithms on the remaining hits, using the track direction from the first iteration. This is illustrated by Fig. 2.10 for the highest multiplicity event.

While a complete analysis of track finding efficiency and acceptance of spurious tracks awaits a complete detector simulation, it is possible to characterize many aspects of the tracking algorithms using data from the test setup. The impact of the second iteration is illustrated in Fig. 2.8. Fig. 2.9 illustrates the mean number of hits per track after the first and second iterations, and the mean number of hits per track not associated with a track.

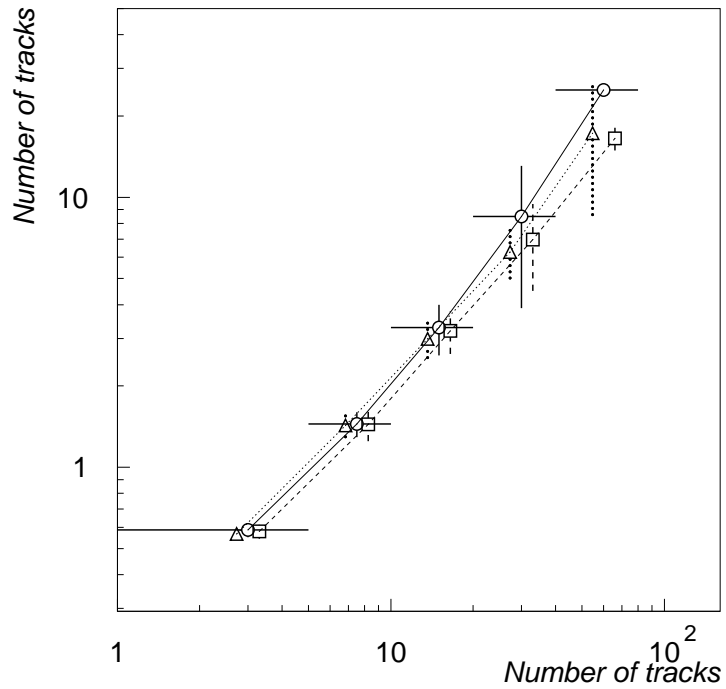


Figure 2.8. Number of reconstructed tracks in the 2nd iteration vs that in the 1st. Circles for 1 mm measurement error, squares for 1.5 mm and triangles for 2 mm.

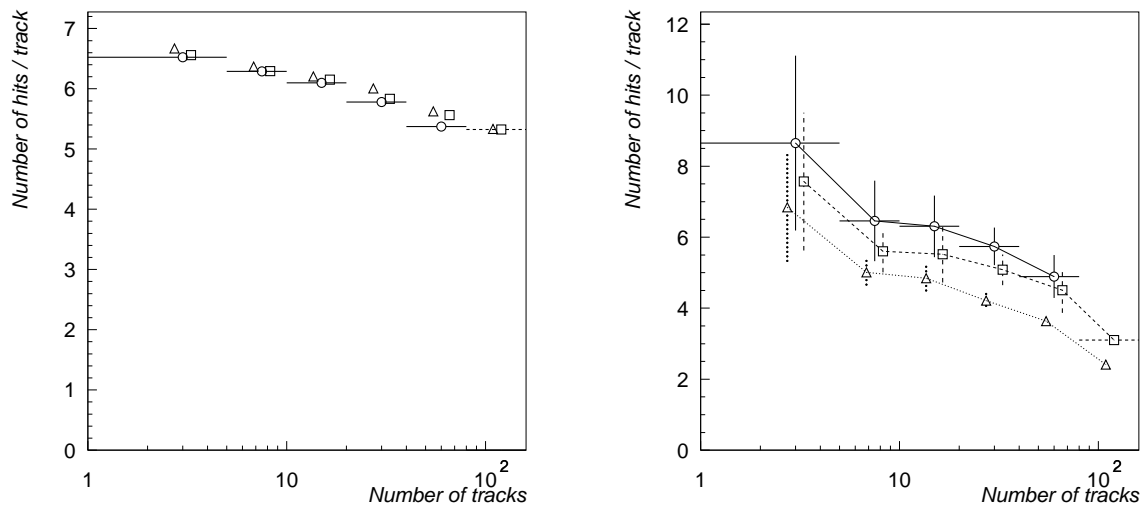


Figure 2.9. Number of used (left) and unused (right) hits per track after the 1st and 2nd iterations. Notations as in Fig. 2.8.

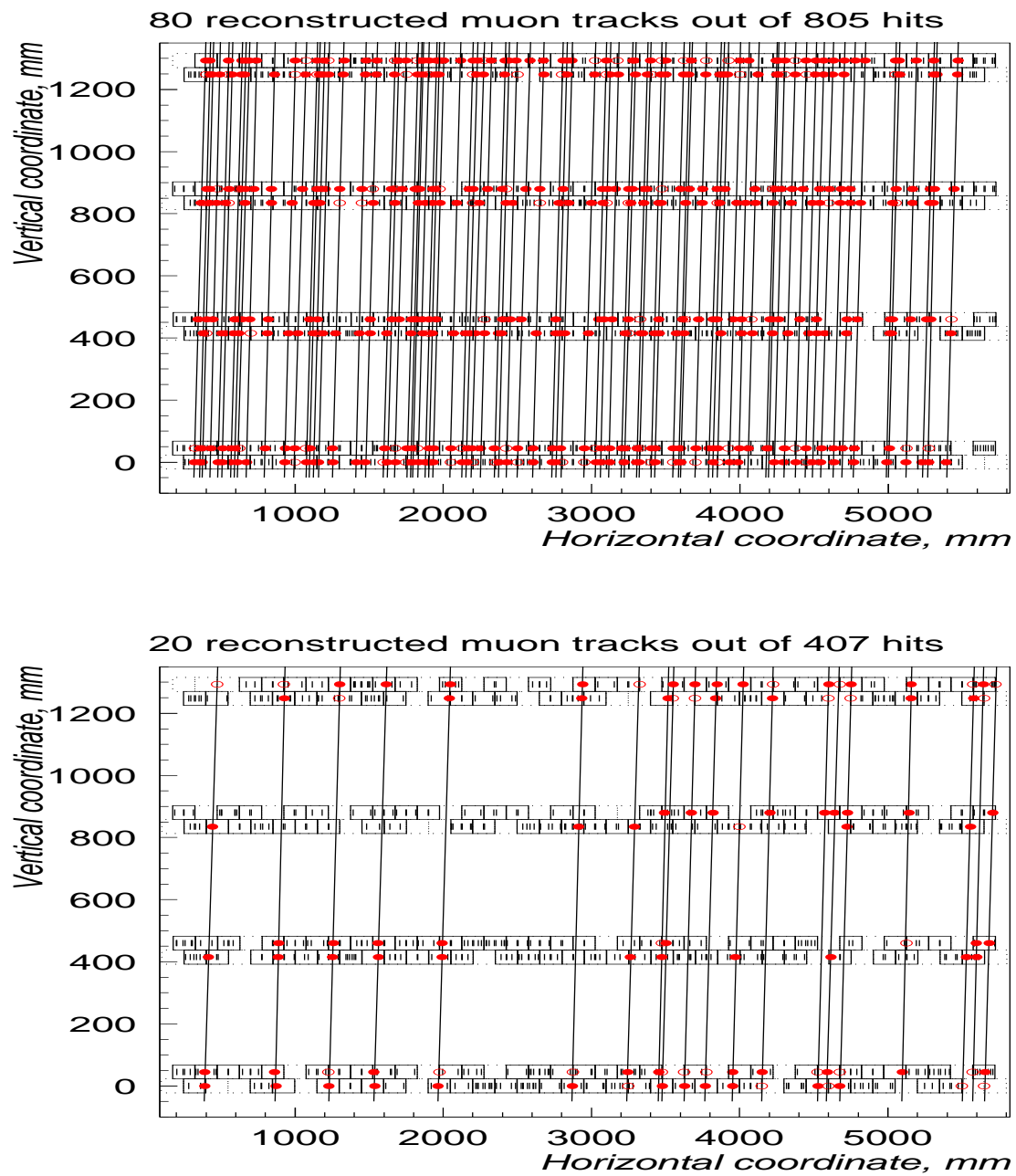


Figure 2.10. The highest multiplicity event found in the test run with the total multiplicity 100 tracks. Top: reconstructed tracks after the 1'st iteration. Bottom: the additional tracks after the 2'nd iteration.

3 The experimental Set-up

We propose two complementary detector arrays:

- an underground array of muon chambers in the LHC cavern I4 at a depth of 140 m, corresponding to a momentum cutoff of 70 GeV for vertical muons, and
- an array of scintillation counters spread over an area of $\sim 20,000 \text{ m}^2$, located on the surface directly above the underground array.

The top array is sensitive to the electromagnetic component of the shower, while the underground array is sensitive to muons coming dominantly from decays of mesons arising in the hadronic component of the shower. The ability to combine the information from the two arrays will provide a powerful tool for the study of high energy cosmic ray air showers in the energy range 10^{14} eV to 10^{17} eV .

The dimensions of the arrays are a-priori given by the available space in the underground cavern, and on the surface, but these are in fact nicely matched to the typical lateral spread of the air showers. For example, the muon density falls by an order of magnitude over a distance of about 15 m, as illustrated in Fig. 1.6. This is well-matched to the 21 m x 23 m size of the underground muon array. On the surface, detectors can be placed on the flat roofs of the buildings and on the surface of the ground with a typical distance between counters of about 10 m. The shower core can be well determined and the energy can be measured by integrating the counter information over a typical radius of 30 to 50 m.

The proposed arrays will permit an increase in statistics by a factor of several hundred over three years, compared to the cosmic multi-muon studies made with the ALEPH experiment. If the five highest multiplicity events observed in the ALEPH detector are not statistical fluctuations, we will have a data sample of about a thousand of such high multiplicity events which will permit a detailed study of their character.

3.1 The underground muon array

The muon array will be installed in the underground cavern of PA4, the former ALEPH experimental region, after the ALEPH detector has been completely removed. No other experiments are foreseen in this intersection region.

It is essential that the platform supporting the muon array be designed in full cooperation with the LHC engineers who are responsible for the installation of the various machine components such as the cryogenics. CORAL must absolutely avoid conflicts with the LHC installation.

Coordination with the LHC has identified the need to maintain two traffic lanes of 4 m width with an effective height of 7 m through the area of the CORAL muon arrays. This will permit suitable access to the LHC tunnel, and will permit other activities on the floor of the cavern. The experiment is restricted to the garage area in order to leave access between the shaft and beam region.

It is therefore proposed to mount the muon array at a height of 7.5 m. The realization of the muon platform, with dimensions of 23 x 21 m² in UX 45 cavern is shown in Fig. 3.1. This platform solution was chosen as it enables the recycling of about 1000 LEP magnets. This will result in a significant cost saving to CERN, for the estimated alternative recycling cost would be about 250 CHF per magnet. The magnets will have to be handled at the surface of point 4 for splitting and temporary storage before they are installed in the CORAL experiment.

The platform is therefore constructed of three piles of magnets, a central and two lateral ones. This arrangement is illustrated in Fig. 3.1. To assure the lateral stability of the construction the three piles are belted by steel sections. The overall stability is warranted by the main beams which form the platform. A part of the steel used is probably provided by other dismantled

structures from LEP.

An axonometric view of the arrangement with the UA1 chambers and the platform construction is given in Fig. 3.2-a and a plane top view in Fig. 3.2-b. The active area of the 9 modules is about 180 m^2 distributed over 400 m^2 . The main beams house the six planes of DELPHI chambers as well as the trigger counters. A new line of LEP magnets is mounted on top of the beams. These will serve as shielding for the DELPHI chambers and at the same time build the platform on which the three UA1 chambers on top of each other are placed (see Fig. 3.3). The shielding thickness amounts to 200g/cm^2 , significantly more than in our test set-up.

In summary, the muons tracks are sufficiently well defined in the short wire projection by 6 planes above and 6 planes below the absorber to determine the muon multiplicity; in the other projection with 6 planes on the top the average muon direction is measured.

3.2 The surface air shower array

To further characterize the cosmic air showers associated with underground muons, it is proposed to install an air shower array on the surface with some 200 scintillation counters, 0.5 to 1 m^2 area each, which are spread over an area of $150 \times 150 \text{ m}^2$. We benefit from experience of other similar arrays such as HEGRA [42] at La Palma, KASCADE at Karlsruhe and the L3C array on the surface above the L3 experiment. In fact, we have obtained all shower counters and associated electronics from the HEGRA and the L3C experiments.

A typical 10^{15} eV air shower deposits most of its energy within a distance of about 30 m from the shower core. Since we aim to trigger on showers with energies above about $5 \cdot 10^{14} \text{ eV}$, and to determine their cores with a precision of better than 5 m, we should locate the shower counters on a grid with a 10 m spacing.

The buildings in the area, which all have flat roofs, and the topography of the land above PA4 are ideally suited for positioning the counters on such a regular grid. Thus many counters can be installed on the top of CERN buildings. Fortunately, the land on the Jura side is relatively flat and at almost the same height as the buildings. Some detectors will be placed on suitable elevated structures in order to prevent the shadowing of detectors by nearby buildings, thus making the array response as uniform as possible. The placement of shower counters over roads or common areas will be avoided.

Fig. 3.4 schematically displays the location of the shower detectors on the CERN property around the LHC pit. Note that surface array is asymmetrically situated with respect to the center of the underground muon array. We are presently investigating the possibility of extending the array by installing counters (indicated by open circles in Fig. 3.4) on land adjacent to the CERN property in order to create a more symmetrical arrangement. Present plans for the experiment, however, assume that the shower counters are located only on CERN property.

There are two basic types of shower detectors that will be used in the shower array. The "HEGRA" type counters (Fig. 3.5) consist of 4 blocks of 50 mm thick plastic scintillators ($25 \times 25 \text{ cm}^2$ each) which are viewed by two photomultipliers located at a distance of 80 cm from the scintillator surface. Scintillators and photomultipliers are enclosed in a light-tight box.

The other type (Fig. 3.6), similar to those used in the L3C experiment, consist of two 10 mm thick plastic scintillators ($25 \times 25 \text{ cm}^2$ each), placed side-by-side in a light-tight rectangular aluminium box. 16 sigma-shaped grooves, 2 mm wide and 2 mm deep, have been machined on the top surface of each scintillator block. 32 wavelength-shifting fibres in the grooves, all of the same length, channel the light to the 50 mm photocathode of a fast photomultiplier.

It is essential to operate the photomultipliers at a high gain in order to ensure single particle detection with high efficiency and an accurate measurement of the pulse amplitude. This, however, restricts the dynamical range to about 100 particles due to the onset of nonlinearity in

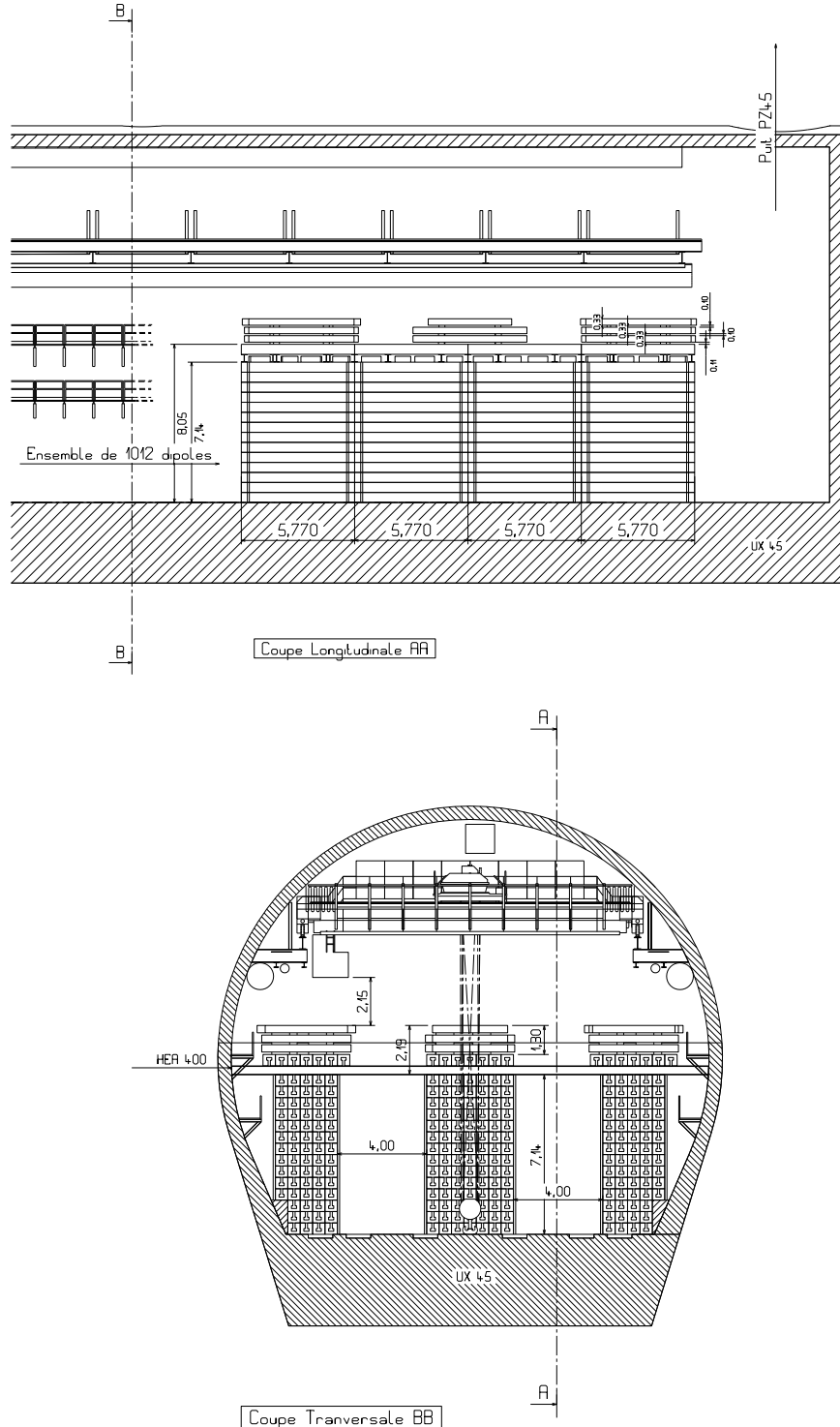
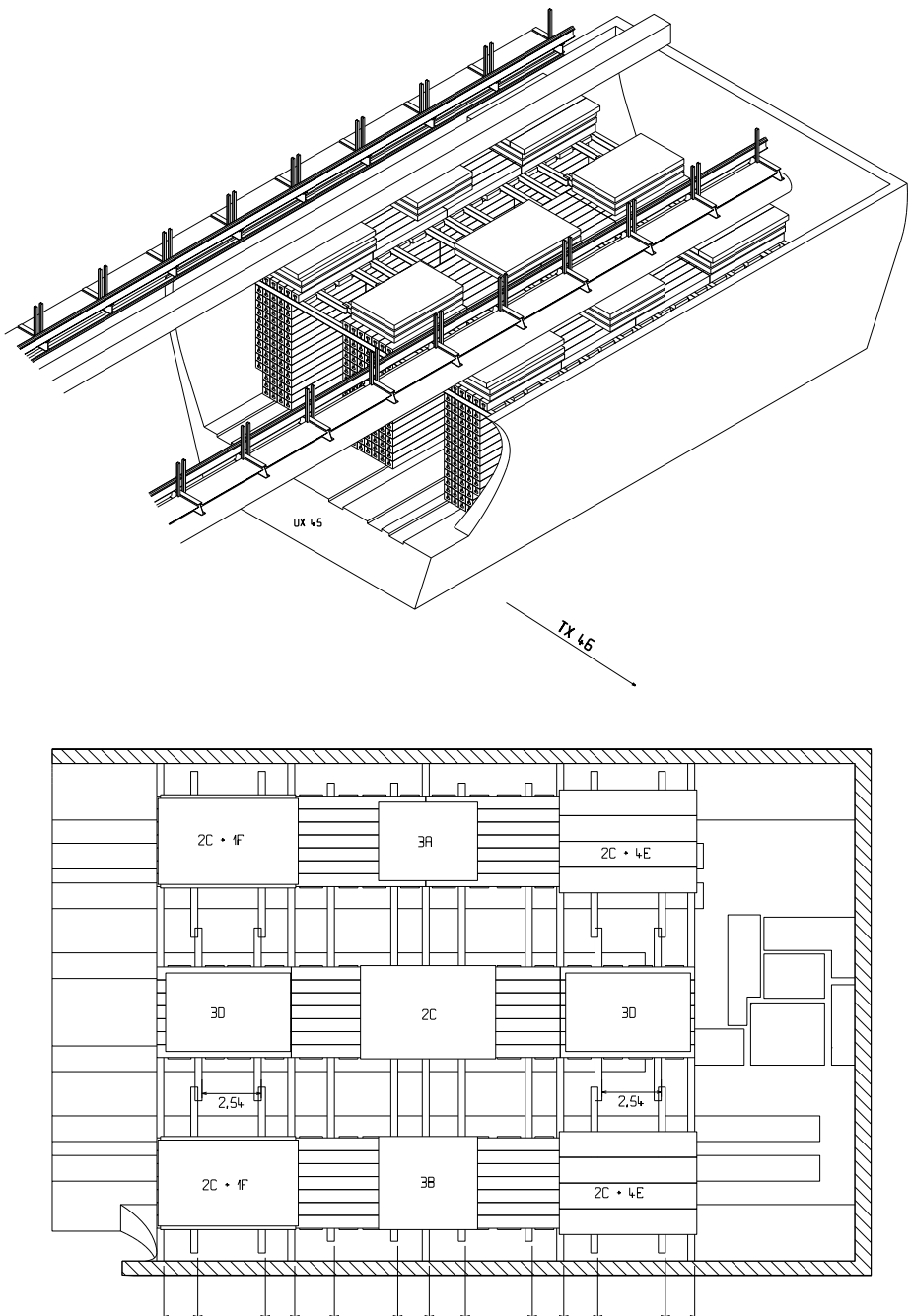


Figure 3.1. The CORAL underground muon array mounted atop platforms constructed of LEP magnets.



[Vue en plan du montage des détecteurs]

Figure 3.2. The underground muon array atop the platform of LEP magnets. (a) axonometric view. (b) plane top view.

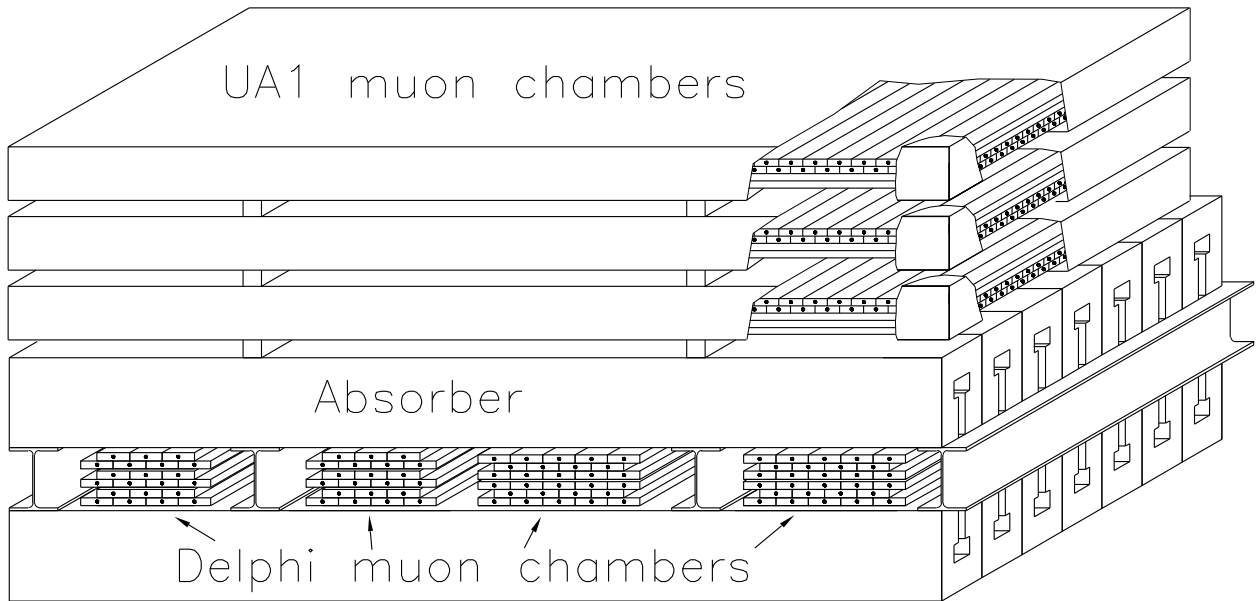


Figure 3.3. The principal set-up of the UA1 and DELPHI chambers with the 200 g/cm^2 absorber in between

the response of large signals. A much larger dynamical range is necessary to make air shower measurements over at least three decades of energy. The detectors are therefore equipped with a second photomultiplier operating at a reduced gain. The 32 fibres are equally shared between the two photomultipliers resulting in a dynamical range of more than 5000.

The detectors have to be calibrated before installation, and on occasion during operation. Before installation, the response of each counter to minimum ionizing particles (mips) can be adjusted by triggering with a small hodoscope on single muons. Fig. 3.7 shows a typical "Landau" like charge distribution obtained with such a measurement. During operation, the mip response can be indirectly gauged using the data of selected small air showers which seldom deposit more than one particle per detector. This calibration method is affected by the large low-energy photon flux and hence is mainly used for a relative calibration.

Some features of our array can be deduced from the performance of the quite similar but smaller (50 counters) surface array which had been operated in the L3C experiment. Fig. 3.8 shows the distribution of the number of counters which have triggered the array. The trigger, which required at least three counters, became fully efficient for 10^{14} eV proton - and $3 \cdot 10^{14}$ eV iron - primaries. Above a counter multiplicity of 10, the distribution follows an exponential law with an exponent of -2.7, in good agreement with the simulation. The distribution of the number of particles, which more closely reflects the energy distribution, is displayed in Fig. 3.9. An energy of 10^{14} eV corresponds to 100 particles. The exponential law is also in good agreement with the simulation. The open circles show the spectrum with at least one muon in the underground array. Above 10^{14} , almost every shower registered on the surface is accompanied by at least one muon underground.

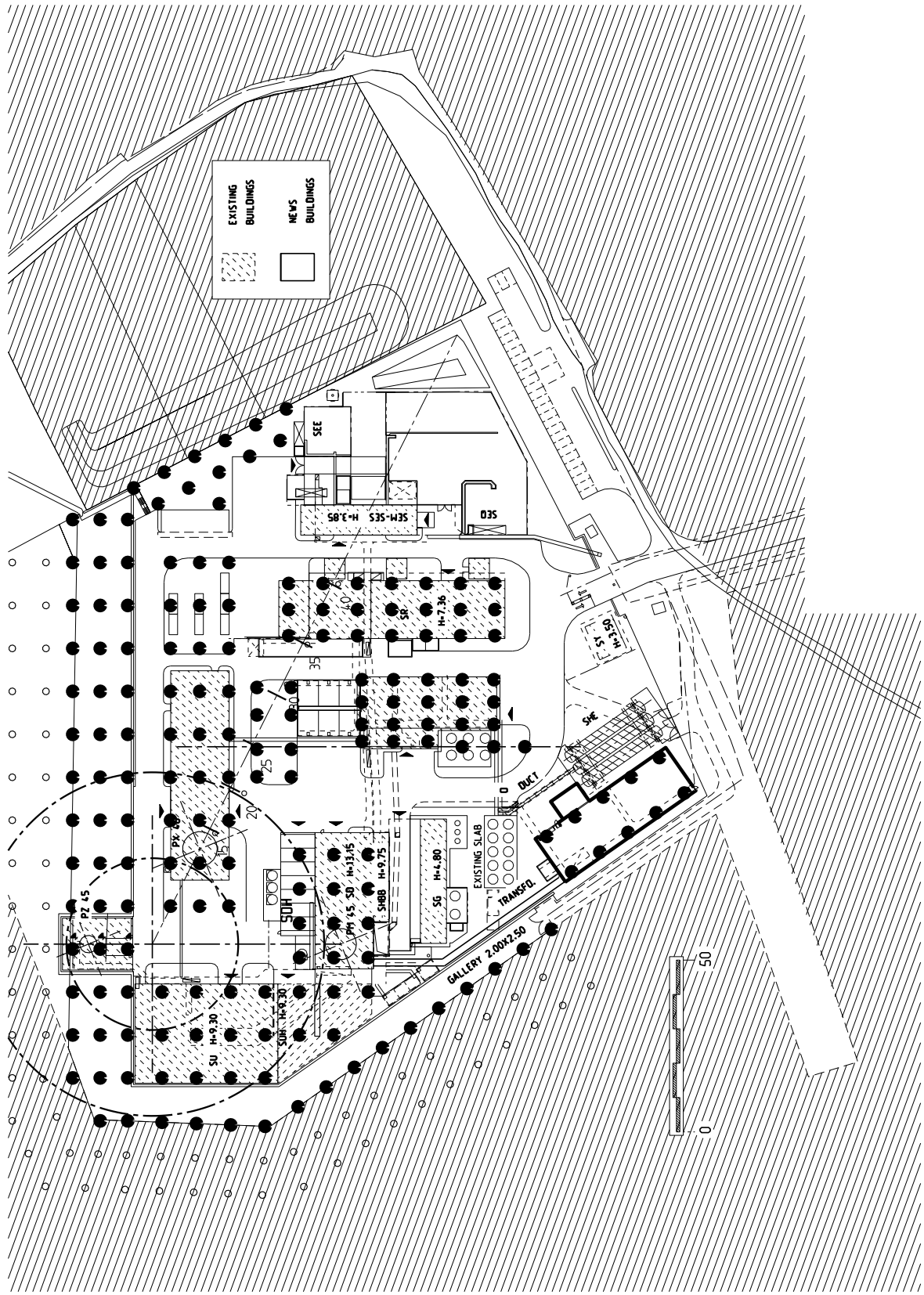


Figure 3.4. The layout of the air shower detectors on the CERN property at PA4. Detectors outside the CERN property are indicated by open circles

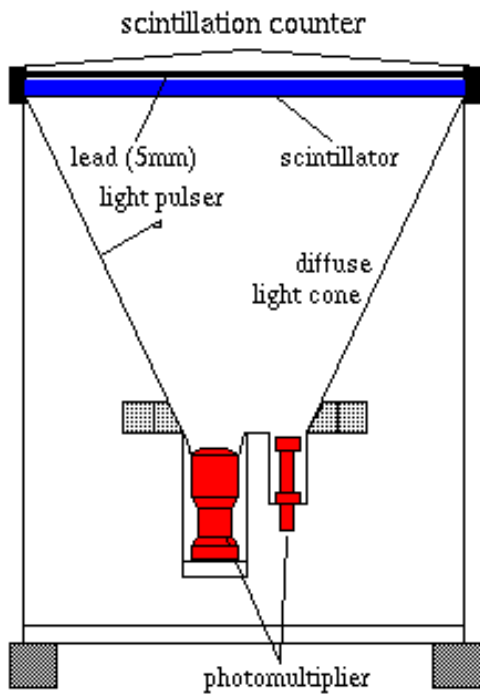


Figure 3.5. The HEGRA detectors.

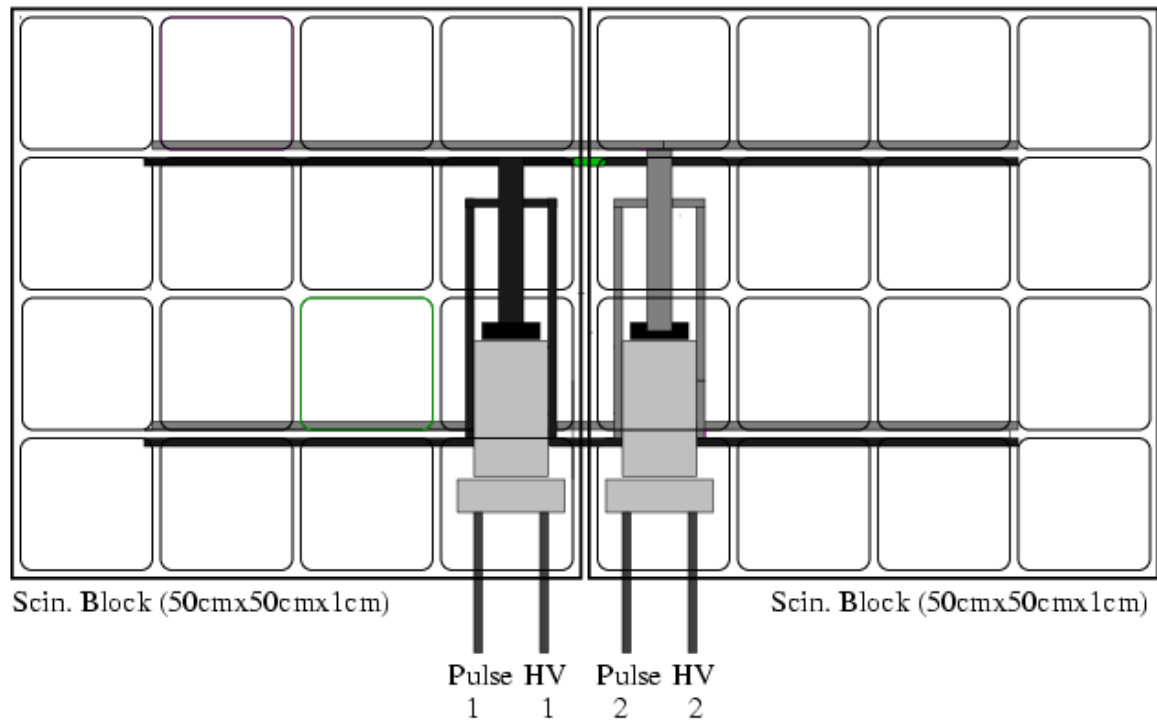


Figure 3.6. The L3C scintillator modules.

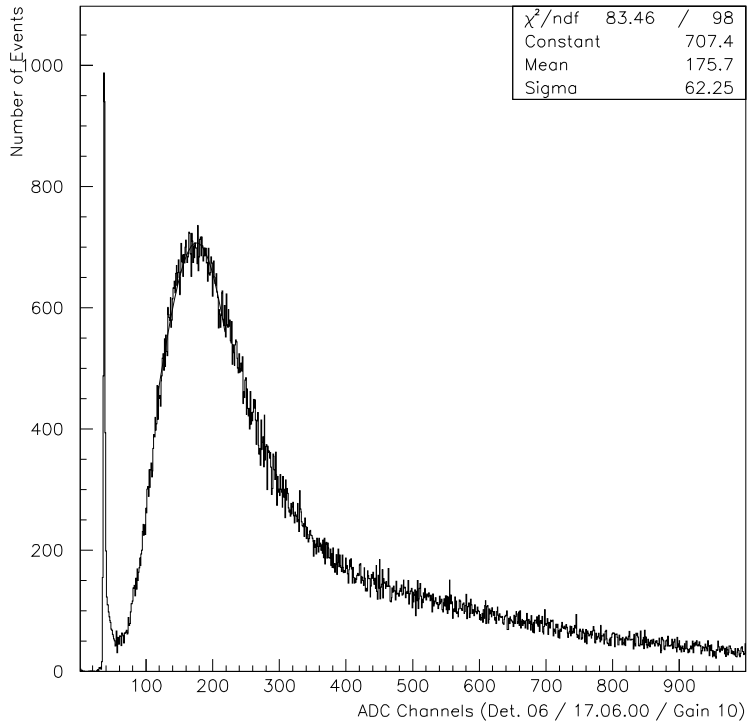


Figure 3.7. Response of the L3C air shower counters to a minimum ionizing particle.

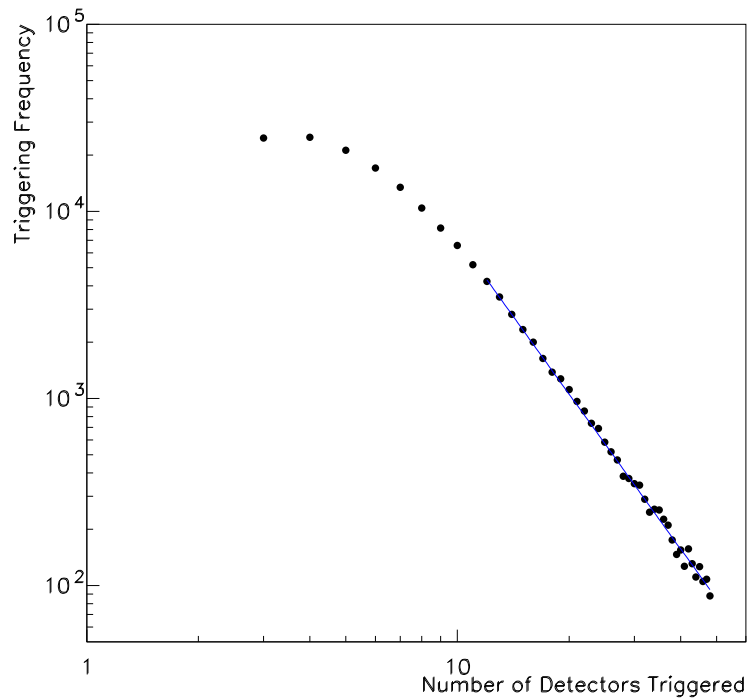


Figure 3.8. Trigger frequency (in arbitrary units) versus the number of hit counters from a 50 counters array above L3.

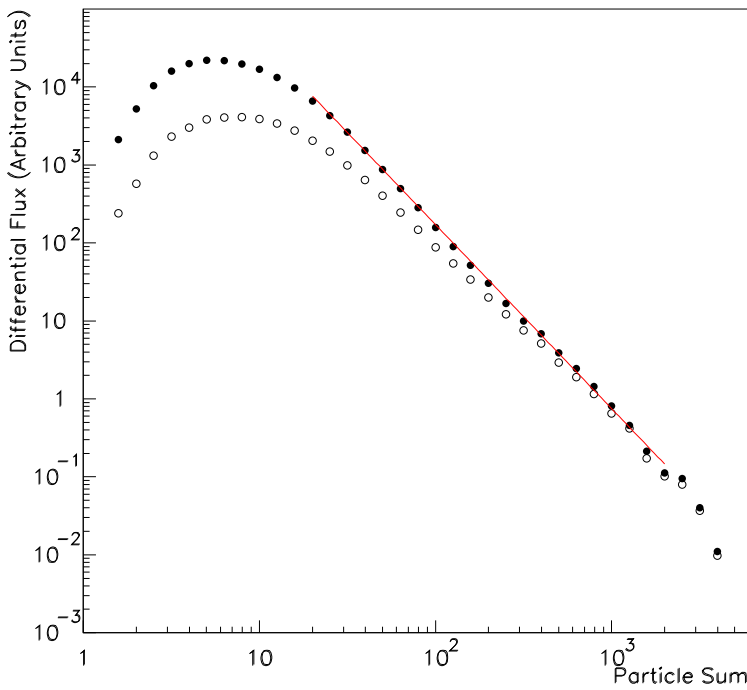


Figure 3.9. Flux (in arbitrary units) versus the sum of all particles, obtained from the pulse heights of the hit counters. The open circles represent events with at least one muon in the L3 muon chambers.

3.3 Trigger

The muon array trigger and the air shower array triggers have to be as flexible as possible so that they can be combined in various ways. The standard trigger must be fully efficient for showers with energies above $5 \cdot 10^{14}$ eV and should not exclude unusual events. For example, AntiCentauro events with a sizeable electromagnetic component and almost no muons should be accepted, as should pure muonic showers with almost no electromagnetic component.

Typical time differences between the various counter elements are given by the spatial distance between them, but also depend on the time difference resulting from an inclined shower front. The information has therefore to be stored for at least $2 \mu\text{s}$. This is straightforward for time measurements since modern TDC's typically can store the information for $64 \mu\text{s}$. ADC pulseheight measurements are slightly more involved.

Cosmic ray trigger rates are low and therefore the read-out and storage of the events do not represent a great challenge. At a primary energy of 10^{14} eV, the surface trigger rate is about 1 Hz for an effective area of the order of 10^4 m^2 , and less than 1Hz for a two-muon trigger in the underground array. A simple “OR” between the top and the underground triggers will probably have the required flexibility.

The underground trigger is made by an n -fold coincidence between a double-layer of counters covering some 20% of the active muon module surface. Photomultipliers are mounted on opposite ends of the $4\text{m} \times 0.2\text{ m}$ counters. Their signals are put into coincidence via mean-timers, yielding a precise timing which is needed for the drift chambers. Varying the value of n corresponds to varying the minimal muon density which will provide a trigger.

The CORSIKA Monte-Carlo has been used to study the performance of the trigger. Fig. 3.10 shows the effect of the n -fold counter coincidence on the primary cosmic ray spectrum. The effective energy threshold increases as n is increased. The trigger curves are given for shower

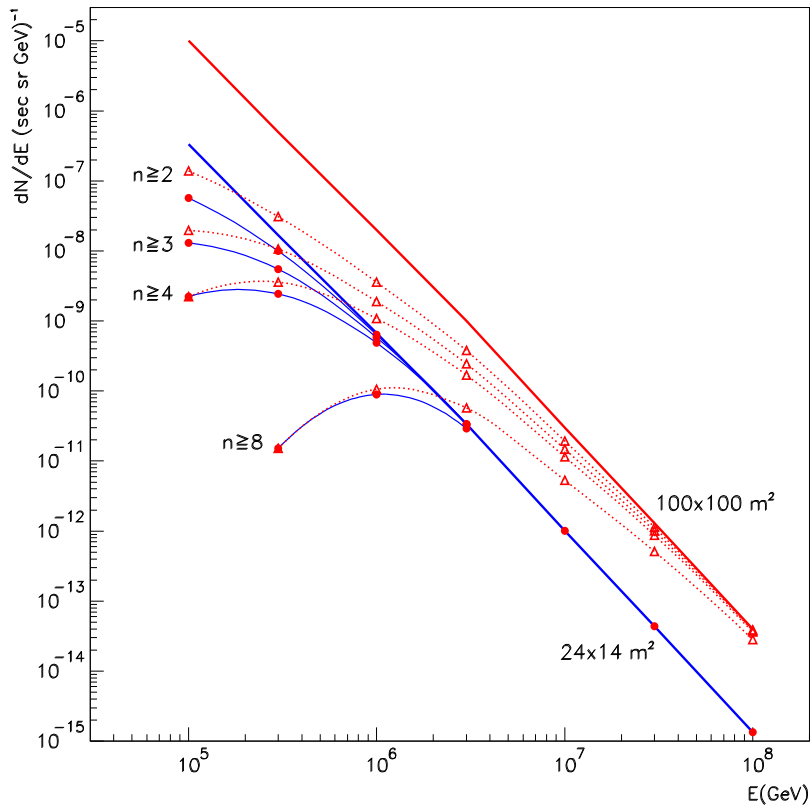


Figure 3.10. The primary cosmic ray energy spectrum for two arrays and the effect of a n -fold coincidence (as described in the text) on it.

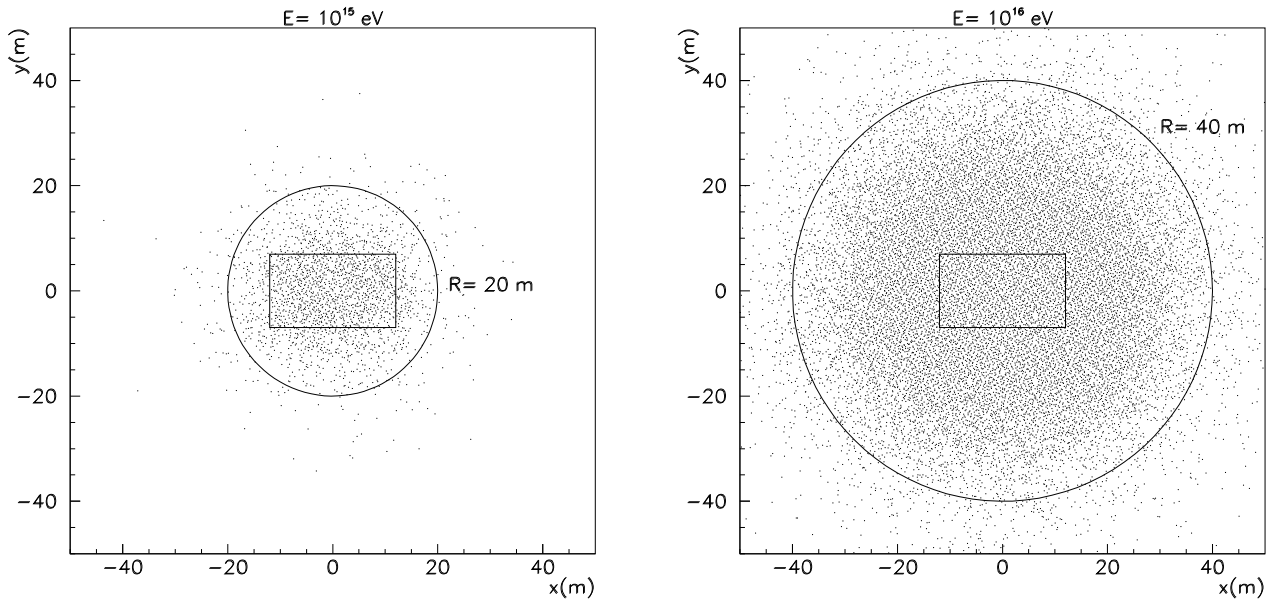


Figure 3.11. Shower core positions with respect to the center of the muon array for two energies and a 4-fold muon trigger coincidence.

cores falling in two different sized regions. As can be seen from the spectrum for the case where the shower core lies within an area of $100 \times 100 \text{ m}^2$, higher energy muon showers can satisfy the trigger condition even when their cores are at larger distances. The higher the energy of the shower, the larger the distance to the muon chambers can be, partially compensating for the lower rates at high energies. For example, the shower core can be in the $100 \times 100 \text{ m}^2$ area for showers with an energy of 10^{16} eV , but it has to be close to the muon chambers for energies around 10^{15} eV . To further illustrate the trigger acceptance, Fig. 3.11 displays the shower core positions for showers satisfying a 4-fold trigger coincidence for two different energies.

The surface trigger consists of a n -fold coincidence of any counters in the area. The value of n has to be chosen such that the surface trigger rate is at most of the order of 10 Hz. From our preliminary calculations and from the experience of the L3C surface array, $n \sim 10$ is a suitable value. This results in an energy threshold due to the trigger of $\sim 10^{14} \text{ eV}$ for proton-induced shower, and three times higher for iron-induced showers. Rather loose trigger conditions have been chosen to be sensitive to unforeseen event topologies. This implies that only a small fraction of the events will be used to determine the particle composition. For this analysis, we require that the shower core lies within 25 m to the center of the underground muon array and is situated at least 10 m inside the boundary of the surface array.

The geometrical acceptance of this configuration is plotted in Fig. 3.12 as a function of the zenith angle. The extended array has about 45% more acceptance than the one restricted to the CERN property: $1100 \text{ m}^2 \text{ sr}$ compared to $750 \text{ m}^2 \text{ sr}$ for zenith angles below 30 degrees. For a data taking time of $6 \cdot 10^7$ seconds, corresponding to 3 years of running, Fig. 3.13 shows the number of events used in the analysis for the particle composition as a function of the primary energy. For the study of the particle composition, more than 1000 events will be accumulated with energies above 10^{16} eV .

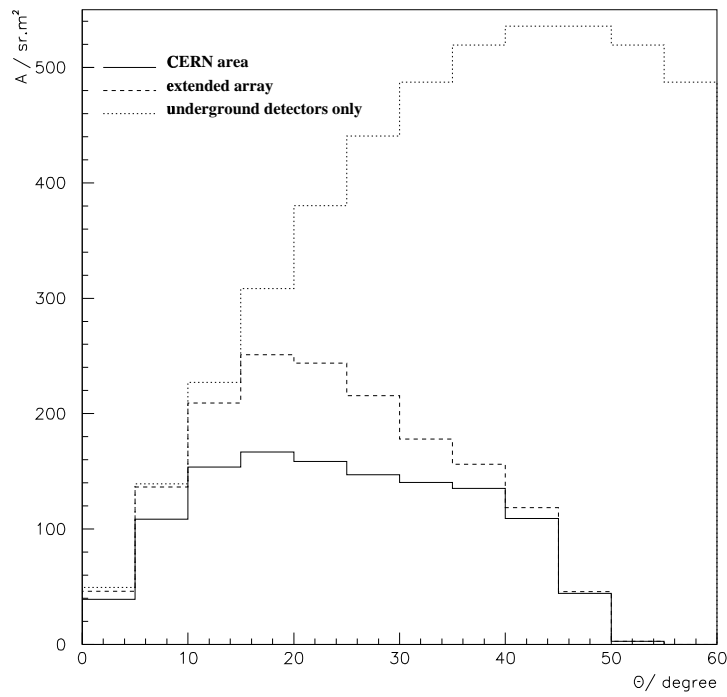


Figure 3.12. Geometrical acceptance of the combined surface - and muon array versus the zenith angle. Note that the top curve corresponds to an infinite surface array.

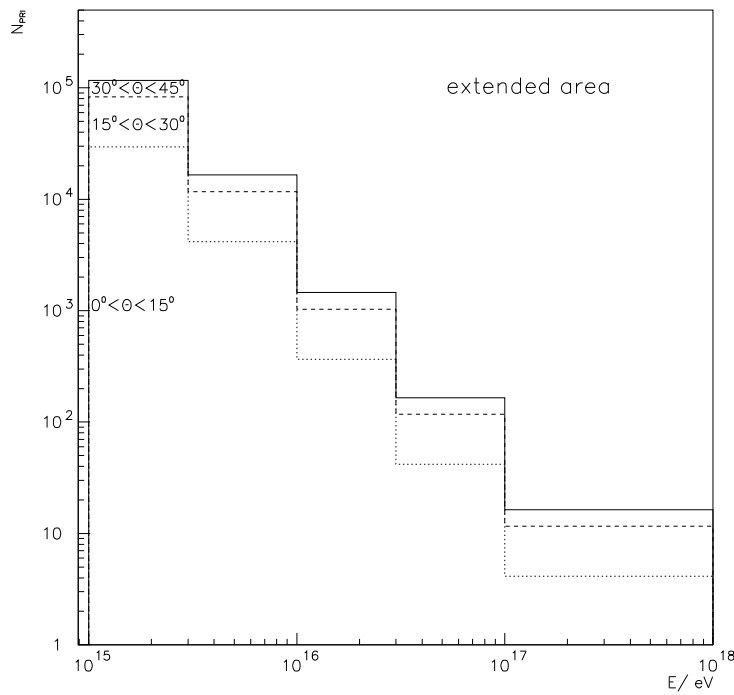


Figure 3.13. Number of events per energy bin, used in the analysis for the particle composition, for a run time of $6 \cdot 10^7$.

4 Monte Carlo studies of detector performance

4.1 The CORSIKA Monte-Carlo

The CORSIKA Monte Carlo [44] has been used to study the performance of the surface air shower array and the underground muon array. CORSIKA (COsmic Ray SImulations for KAscade) is a detailed Monte Carlo program developed to study the evolution of extensive air showers initiated by a variety of different primary cosmic rays down to the observation level. The program includes a number of different interaction models. The results presented here are based on the QGSJET model.

In order to optimize our use of these very computation-intensive Monte-Carlo simulations, two different samples of air showers have been generated by CORSIKA used, one for studies of the performance of the underground array alone, and the other for studies including the performance of the surface array. The difference lies in the fact that the underground array is only sensitive to muons, and hence the electromagnetic component of the air shower can be neglected, leading to very significant savings in computation time. On the other hand, studies involving the surface array, which is sensitive to the electromagnetic component of air shower, requires a full simulation of the air shower, at a significant cost in computation time.

For the analysis of the underground array alone, events were generated with both proton and Fe primaries. The energy interval $10^{12}\text{eV} < E < 10^{18}\text{eV}$ was divided into two bins per decade, and 1000 events were generated within each bin, except for the highest energy bins, where only 500 events were generated in each bin due to the large computation times required. The zenith angle θ was randomly distributed over the interval $0 \leq \theta \leq 60^\circ$. The events were then weighted according to the actual cosmic ray spectrum. The shower axes were uniformly distributed over an area of $200 \times 200 \text{ m}^2$ centered on the muon array, and the muons hitting the chambers were recorded. A momentum cut of $70 \text{ GeV}/\cos(\theta)$ was applied to account for energy loss in the rock overburden. (See Appendix A for a more detailed discussion of the muon energy cutoff.)

As noted above, a full simulation of the air showers is necessary in order to study the performance of the surface air shower array together with the underground muon array. Fortunately, the KASCADE collaboration has kindly provided with their air shower simulation data sets. Events were generated for both proton and Fe primaries. The energy interval $5 \cdot 10^{14} \text{ eV} \leq E \leq 5 \cdot 10^{16} \text{ eV}$ was divided into 4 bins per decade. An $E^{-1.5}$ energy spectrum was used. This permits efficient generation of events with good statistics over the energy range; the events can be weighted to account for the steeper cosmic ray spectrum. The events were generated with zenith angle θ in the range $0 \leq \theta \leq 42^\circ$. The showers were analyzed at an elevation of 110 m above sea level. A correction factor accounting for the higher elevation of the CORAL experiment has to be applied. A total of ~ 1800 events in this data set were used in our analysis.

Electrons, muons and hadrons hitting the sensitive area of the surface air shower array were registered. Muon propagation to the underground array was modelled by using the same energy threshold discussed above. Muons surviving the cut and hitting the sensitive area of the underground array were registered. A trigger condition of $N_\mu \geq 2$ was imposed. (An extensive study of trigger conditions for the underground array was studied in [1]; these results remain relevant here.)

4.2 The underground muon array alone

The proposed muon chamber array will permit the study of the structure of multi-muon events. The core position and the primary energy can be determined provided that the shower core falls within or close to the array. Proton and iron induced showers can be distinguished, at least on a statistical basis, from the structure of the muon bundles. Indeed, we have already

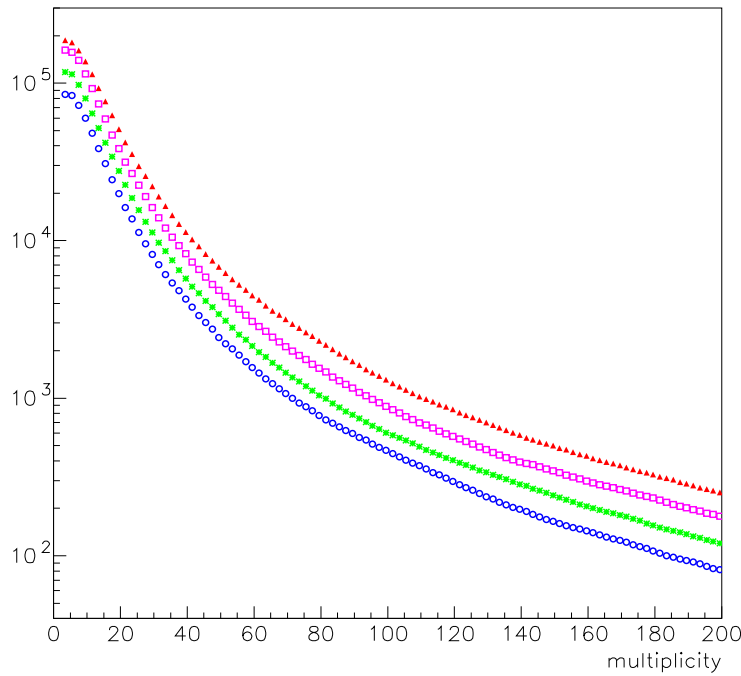


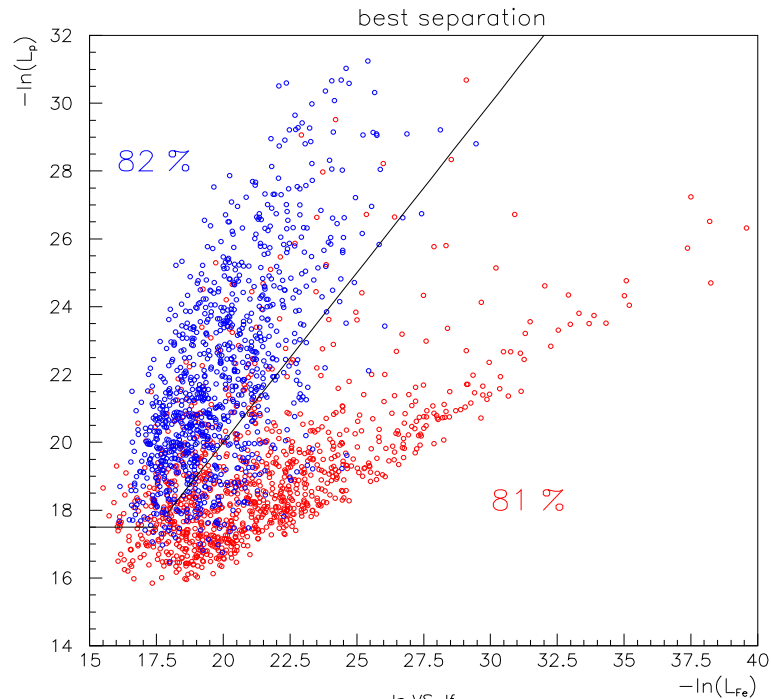
Figure 4.1. The integral muon multiplicity distributions in the underground array for different primary particles for a running time of 2·10⁷ sec.

observed a transition from proton to iron induced showers at high multiplicities within the limited statistics of the data obtained with the ALEPH detector. The equivalent integral inclusive muon multiplicity distribution for the new CORAL underground muon array is given in Fig. 4.1 for the four primaries (p, He, O, Fe). Assuming a measurement time of 2 x 10⁷ seconds, the new data set will be 100 times larger and will thus permit further, more detailed, study of the primary composition. If the primary distribution becomes heavier with increasing energy (and hence multiplicity), the measured distribution should shift gradually from the lower to the upper curves with increasing multiplicity. Similarly, if the high-multiplicity excess seen in the ALEPH TPC would persist we should observe about 1000 events with these high densities, a good sample for the study of their properties.

As already demonstrated in the CosmoLep proposal [1], the position of the shower core can be reconstructed from the muon distribution in the chambers with an accuracy of a few meters if it falls within the array. Once the shower core is determined, the radial muon density distribution can be used to estimate the primary particle type and to determine the primary energy from the central muon density which is almost independent of the particle type (see the radial density distribution in Fig 1.6). The fact that the radial distribution is considerably flatter for iron-induced muon bundles is the key to discriminating between proton and iron-induced showers.

The identification of proton and iron primaries on an event-to-event basis is difficult. For a given core position and for different energies, a normalized multiplicity distribution in each chamber is simulated for proton and iron primaries. The multiplicities are then rescaled so that the average multiplicity in the core is the same for proton and iron induced showers. In this way, the identification is only based on the radial distribution. These masks for each chamber

$E = 3 \times 10^{15}$ eV – red=p data – blue=Fe data / all chambers



$E = 10^{16}$ eV – red=p data – blue=Fe data / all chambers

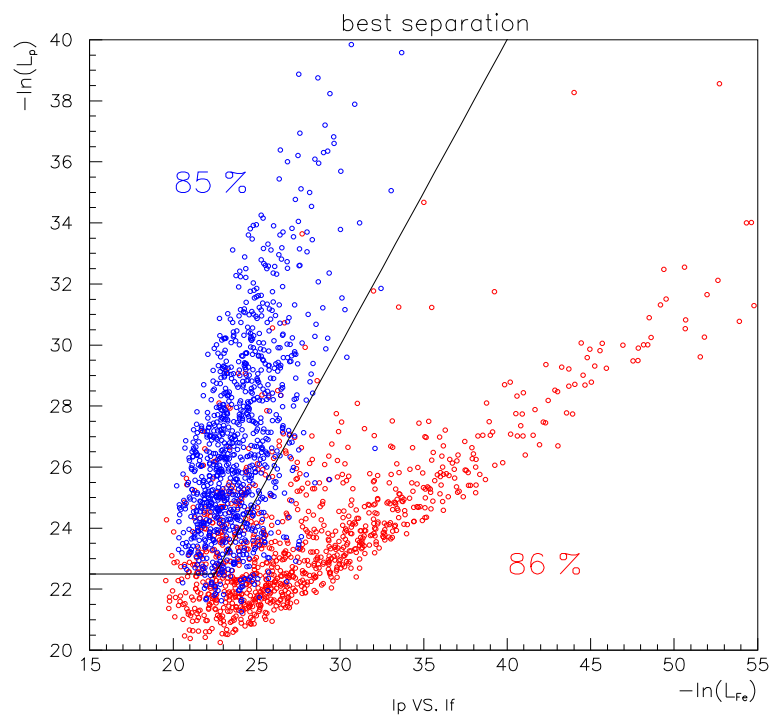


Figure 4.2. $-\ln(L_p)$ vs $-\ln(L_{fe})$, where $L_{p(fe)}$ is the likelihood, for a proton (iron) sample. The fraction of correctly identified events refer to the cuts shown in the plots.

are then applied to the individual events and a likelihood is calculated for the proton and the iron assumption. Fig. 4.2 shows a two-dimensional plot of these two likelihood values per event. Separating the two distributions by the indicated lines, we are able to identify correctly 86% (81%) of the protons and 85% (82%) of the iron for 10^{16} eV ($3 \cdot 10^{15}$ eV).

Assuming the particle type has been estimated and the shower core is known, the primary energy can be calculated from the total number of muons in the array. The total muon number, N_{TOT} , rises almost linearly ($N_{TOT} \sim E^{0.9}$) with energy as can be seen from Fig. 4.3. The indicated error bars present the fluctuation of a single measurement. For the same total multiplicity, the reconstructed energy for iron primaries would be 40% lower than for protons. Considering only the muons in the chamber which contains the shower core, the difference would be reduced to 25%. On average, the error in the energy determination is about 25% for proton and better for iron, with only a slight dependence on energy.

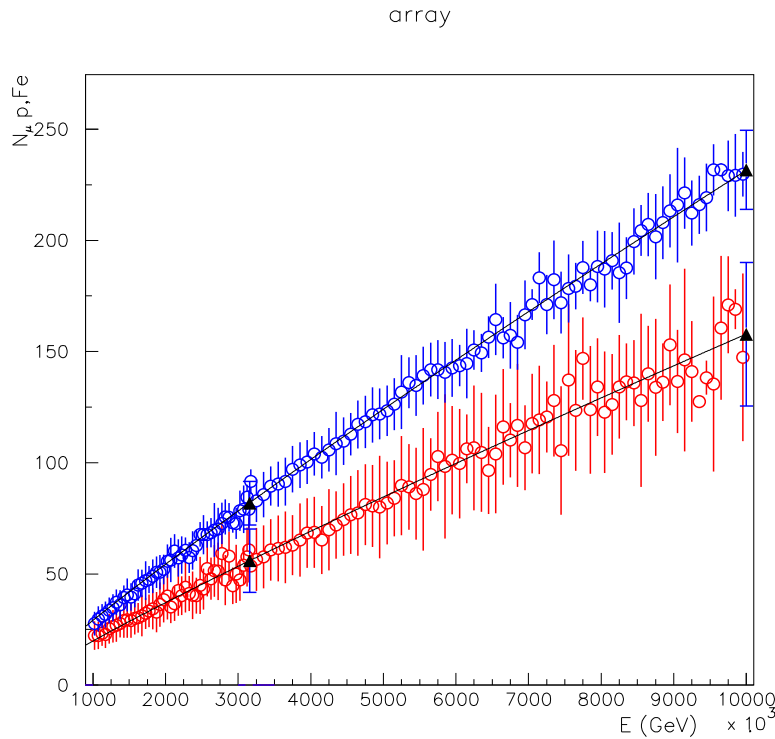


Figure 4.3. Number of muons (N_{tot}) in the array as function of energy, for p and Fe . The black triangles refer to simulation at fixed energy. The fit through these points is also shown (top curve: iron; bottom curve: proton).

4.3 Combined air shower and underground muon array

The surface air shower array will be a powerful tool for the study of the electromagnetic structure of air showers. In this section we focus on simulations illustrating the power of the combined air shower array and underground muon array for the determination of the primary particle type.

The surface air shower array can be used to accurately determine the location of the shower core. This can be done by projecting the distribution of particles onto the two principle axes, as illustrated in Figure 4.4. The accuracy of the determination, ~ 3 m, is indicated in Figure 4.5,

which plots the distribution of the residuals for proton induced showers with energies 10^{15} eV $\leq E \leq 10^{16}$ eV and zenith angles less than 30° . This is comparable to the precision with which the underground muon array can identify the location of the shower core, and is particularly useful for those events in which the core is near, but not within, the underground array.

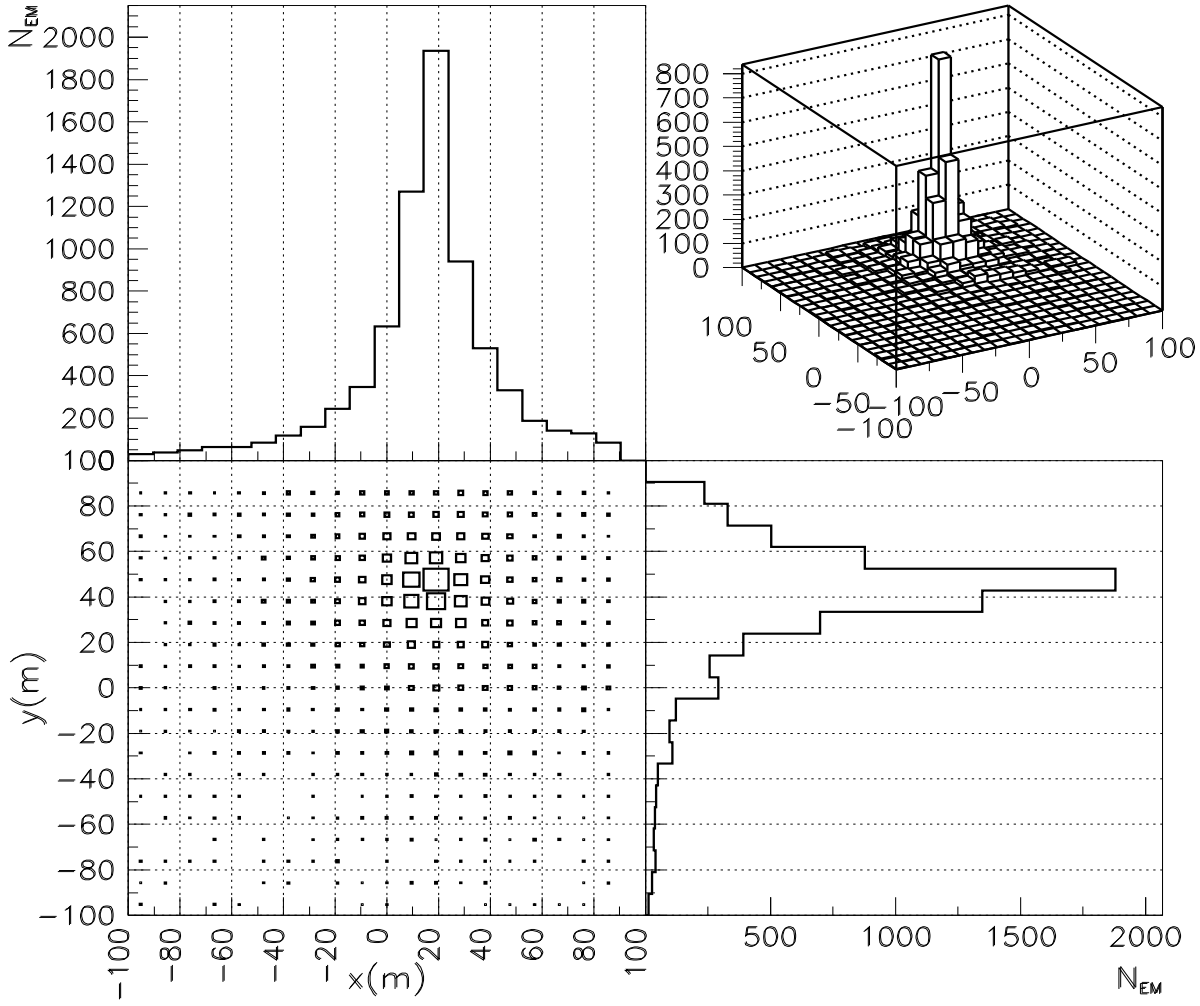


Figure 4.4. Distribution of the electromagnetic particles in the air shower array for one event ($\theta=6^\circ, E=9 \cdot 10^{15}$ eV: the projections on the axis are used for the core determination).

Information from the two arrays can be combined in order to determine the composition of cosmic ray primaries. The basic idea is to use the underground array to measure the number of muons in each shower, and the surface array to measure the number of particles in the electromagnetic component of the shower. Because of the difference in the multiparticle production of primaries of various species, heavier primaries will be relatively richer in muons and relatively depleted in terms of the number of electrons and gamma rays, thus permitting discrimination between, for example, proton and Fe primaries.

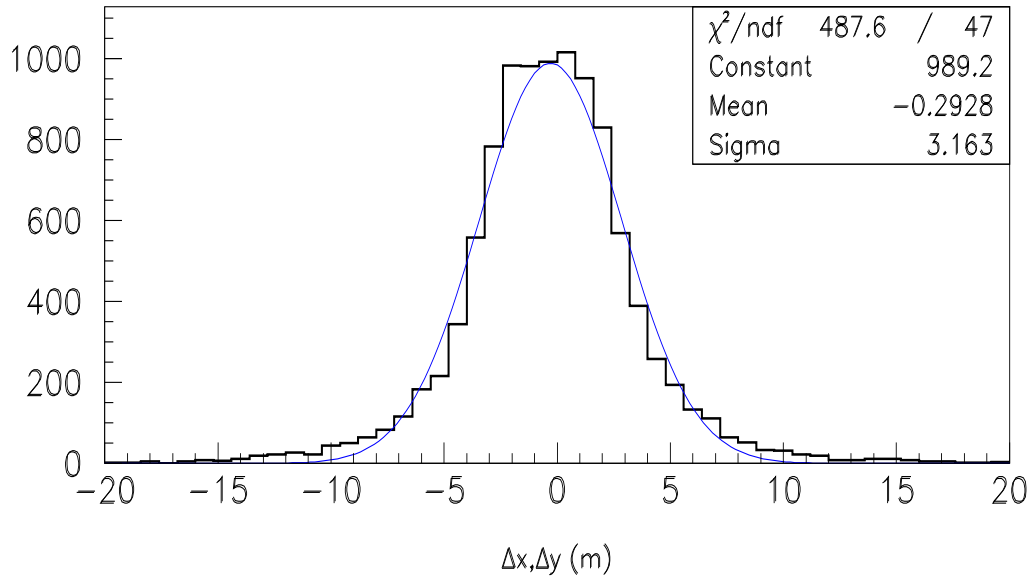


Figure 4.5. The difference between the real and the estimated position for proton induced showers, with $\theta < 30^\circ$, and energy between $10^{15} - 10^{16}$ eV.

Figure 4.6 and Figure 4.7 illustrate the power of the CORAL detector for these studies.

For showers with a zenith angle of less than 15° and whose core lies within 25 m of the center of the underground muon array, there is always a 100×100 m² region of the surface array centered on the shower core at the surface. In Figure 4.6, the total number of particles seen by the surface array counters in this region are summed, and plotted against the number of muons observed by the underground array for events with energies $5 \cdot 10^{14}$ eV $\leq E \leq 5 \cdot 10^{16}$ eV, zenith angle less than 15° , and whose core passes within 10 m of the center of the underground muon array.

For showers with larger zenith angles, $15^\circ \leq \theta \leq 30^\circ$, it is not always possible to find a 100×100 m² region of the surface array centered on the shower. Thus the detection region was reduced to 60×60 m². In Figure 4.7 the separation plot is shown for events with energies 10^{15} eV $\leq E \leq 10^{16}$ eV and zenith angles between 15° and 30° using this reduced area.

The separation of the plots into distinct regions populated almost exclusively by either protons or Fe initiated events is quite clear, and a variety of statistical methods, such as the KNN method, can be used to analyze actual events. Here we present a straightforward method which clearly indicates the power of the CORAL detector.

In Figures 4.6 and 4.7, it is clear that the separation between the regions populated by protons and by iron induced primaries is quite linear. Note that energy increases along the separation line while particle mass changes along the perpendicular axis.

The events plotted in Figures 4.6 and 4.7 had shower cores passing within 10 m of the center of the muon array. In order to extend this region to a radius of 25 m, the radial dependence of the muon density must be taken into account. For larger core distances, the separation line moves downwards to smaller multiplicities, but the p-Fe separation stays almost same for different radial distance intervals. Correcting for this radial dependence, we can extend the minimum shower core distance from the center of the muon array from 10 m to 25 m.

Projecting events onto the axis perpendicular to the line of separation yields the distributions of Figure 4.8-a. If one discriminates between proton induced events and Fe induced events by

cutting on this distance perpendicular to the line of separation, some events of each type will be misclassified. This is illustrated in Figure 4.8-b. Note that with judicious choice of the cut, approximately 93% of each species will be correctly identified in the energy range 10^{15} eV $\leq E \leq 10^{16}$ eV. Figure 4.8-c illustrates the dependence of this accuracy on the energy of the primary.

As noted above, it is necessary at large angles to use smaller areas of the surface array to determine the electromagnetic component of the air shower. It is thus useful to define smaller groupings of surface array detectors centered on the surface location of the shower core. These groupings are illustrated in Fig. 4.10. Figure 4.8-b also illustrates the accuracy in discriminating between proton and Fe induced showers for several of these groupings. Figure 4.9 extends these studies to larger zenith angles, $15^\circ \leq \theta \leq 30^\circ$.

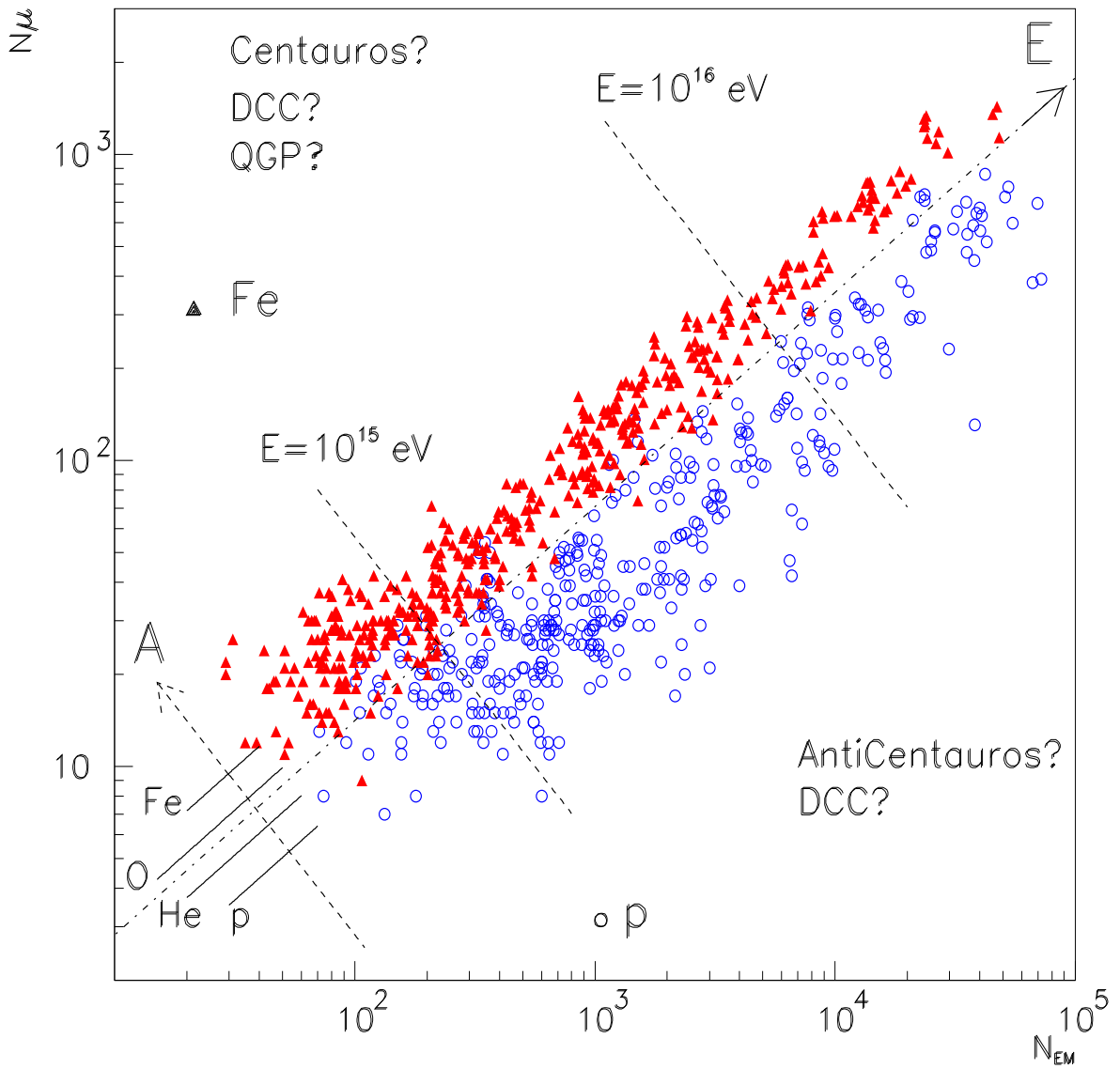


Figure 4.6. Number of muons ($p > 70$ GeV) versus number of electromagnetic particle in an area of 100×100 m 2 , for proton and iron initiated showers, pointing to the center of the underground array within 10 m ($5 \cdot 10^{15} < E < 5 \cdot 10^{16}$, zenith angle $\theta < 15^\circ$). The primaries (p, He, O, Fe) cluster around the straight lines indicated in the plot.)

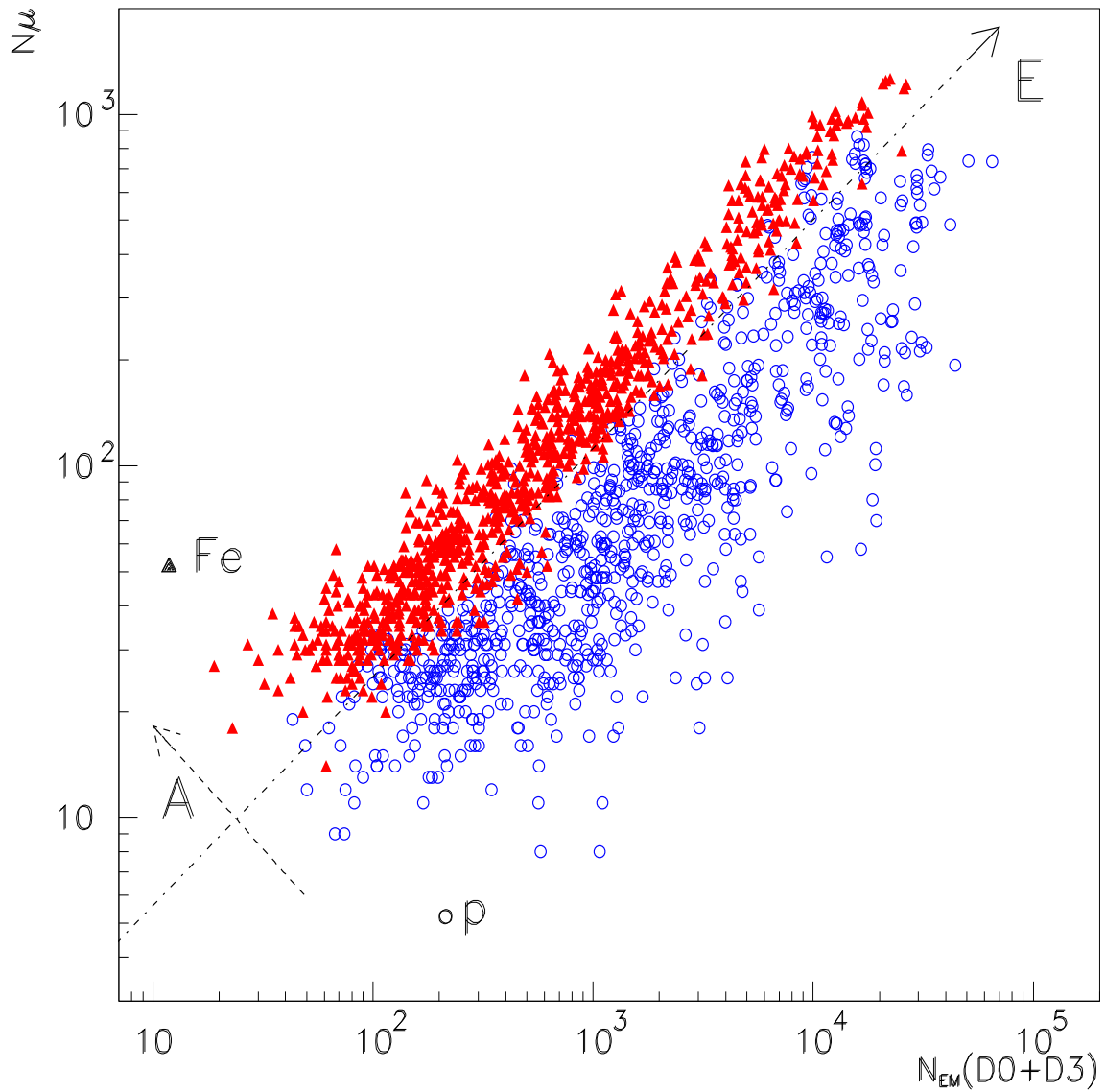


Figure 4.7. Number of muons versus number of electromagnetic particle in an area $60 \times 60 \text{ m}^2$, shower cores at a distance $R < 10 \text{ m}$, $10^{15} < E < 5 \cdot 10^{16}$, $15^\circ < \theta < 30^\circ$

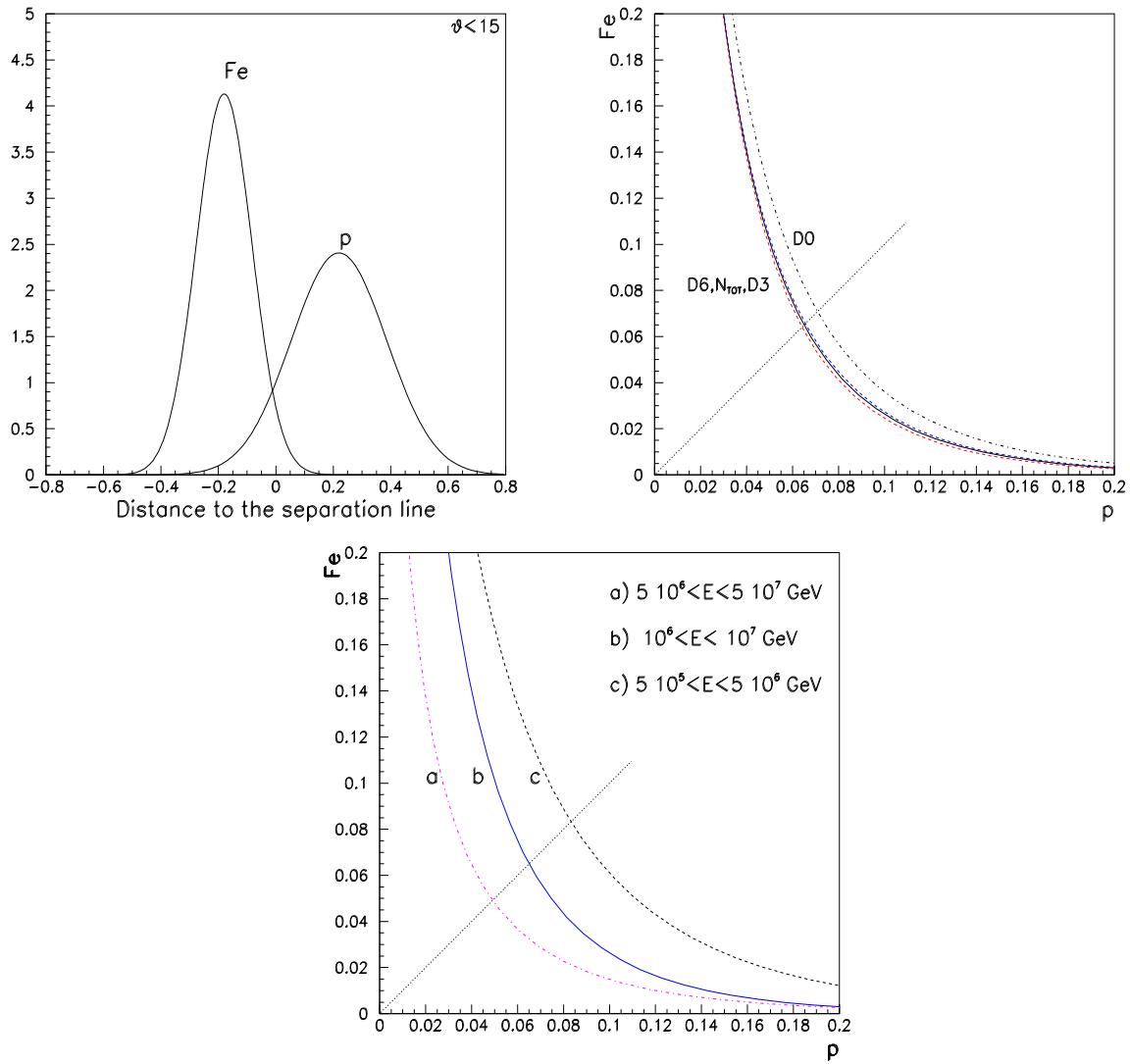


Figure 4.8. From the top and the left: example of two (normalized) distributions of the distance to the separation line considering the number of electromagnetic particles in an area $100 \times 100 \text{ m}^2$ for $\theta < 15^\circ$, shower cores at a distance $R < 25\text{m}$ and $10^{15} < E < 10^{16}$; percentage of misidentified events for different groups of detectors; misidentified events for different energy ranges

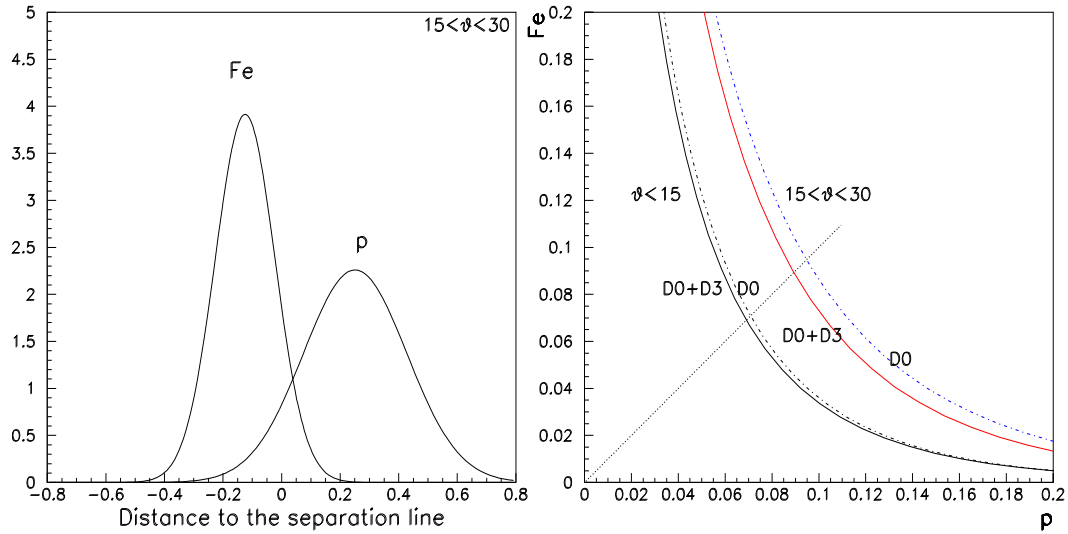


Figure 4.9. From the left: example of two (normalized) distributions of the distance to the separation line considering the number of electromagnetic particles in an area $60 \times 60 \text{ m}^2$ (“D0”+“D3” groups) for $15^\circ < \theta < 30^\circ$ and $10^{15} < E < 5 \cdot 10^{16}$; comparison of the percentage of misidentified events for the two θ ranges considered.

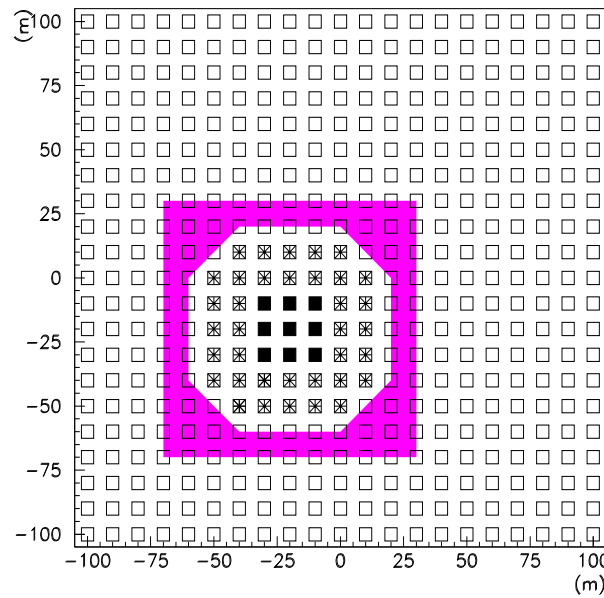


Figure 4.10. The different groupings of surface array detectors defined relative to the core of large zenith angle showers: “D0” - solid; “D3” - asterisk; “D6” - shaded.

5 Schedule

The CORAL experiment proposes to install an underground muon array in the cavern at PA4 and a surface air shower array on the CERN property directly above. A major theme of this proposal is that the depth of the cavern at PA4 corresponds to a particularly interesting and useful cutoff on the muon momentum. Further, the surface at PA4 is ideally suited to an air shower array since there are many accessible buildings with flat roofs, and the ground on the Jura side is at almost the same height as the roofs of these buildings. Further, since PA4 is the former ALEPH experimental area, we will be able to benefit from the superb experimental hall and infrastructure, as well as important technical installations such as the air extraction system.

The CORAL installation schedule is necessarily constrained by the schedule for the removal of the ALEPH experiment, and by the installation schedule of the LHC. We therefore began discussions with LHC planning officers and engineers at an early stage in the preparation of this proposal. These discussions have been very fruitful, and have not revealed any major difficulties in the cohabitation of CORAL with LHC construction at PA4. Indeed, many important aspects of the CORAL proposal, such as the construction of the underground muon platforms out of LEP magnets, originated on the LHC side of our discussions.

The discussions have, however, resulted in a clear understanding of certain boundary conditions. These include the need for CORAL to install the underground array in the so-called garage position, the need to leave the access from the shafts to the machine completely free, and the need to provide two corridors, each 4 m in width and 7 m high, through the experimental area. These constraints are met by the present proposal.

If accepted in the first half of 2001, we will immediately begin construction of the air shower array. A first test experiment can be performed in 2001 if we can install a few dozen counters on the roofs of some of the buildings and put them in coincidence with the existing L3C surface array.

The construction of the platform for the underground muon array can commence after the completion of some civil engineering work for LHC which will reinforce the walls on the Jura side. The first muon chambers can thus probably be installed in the spring of 2002 after they have been carefully tested in one of the halls on the surface.

The complete underground and surface arrays should be commissioned in the summer of 2002 and become fully operational shortly thereafter. This will leave some three years of data taking before the LHC begins operation.

6 Budget

The proposed experiment would have required a budget of many millions of Swiss Francs if newly constructed. These costs are dramatically reduced, however, by using existing detectors and electronics and the CERN infrastructure, particularly the underground cavern at PA4. We are also fortunate that we have inherited the complete air shower array from the HEGRA experiment, as well as the UA1, DELPHI and OPAL muon drift chambers and scintillation trigger counters.

It is our understanding that CERN cannot invest a substantial amount of manpower into CORAL. The manpower is therefore mainly supported by the collaborating institutes. Some funds in addition to the hardware will, however, be needed for subsistence allowances at CERN and for a project associate.

We have found additional collaborators since our CosmoLep proposal in 1999. Negotiations with collaborating institutes have already begun and will continue during the approval phase of the experiment. We are confident that the collaborating institutes will assume responsibility for a fair share of the investment and running costs. It should be noted, however, that some of the participating institutes have already contributed manpower and material.

The estimated budget for the installation of the CORAL experiment and its running is given in Tab. 6.1 together with a breakdown of the budget over the next several years.

	Years: 2001	2002	Total
<u>Underground muon array</u>			
Infrastructures at I4,experimental platform, etc	-	120	120 KFS
Installation of all (UA1+DELPHI) muon chambers, gas system and safety cables and connectors, repairs	80	150	230 KFS
Trigger counters underground (cables, connectors, infrastructure, repairs)	30	30	60 KFS
Trigger logic, GPS	15	80	95 KFS
DAQ, Data storage	30	60	90 KFS
<u>Surface detector array</u>			
Construction and repair of ~200 counters	50	60	110 KFS
Cables, controls....	40	40	80 KFS
Trigger logic,DAQ, GPS	40	50	90 KFS
Maintenance	20	20	40 KFS
Total	305	610	915 KFS
<u>Consumption:</u>			
Rental fee for electronics	50	80	130 KFS
Gas consumption	20	40	60 KFS
Investments and maintenance for the years ≥ 2003			
	2003	≥ 2004	
Upgrades	60	-	KFS
Maintenance	60	60	KFS
Rental fee for electronics	80	80	KFS
Gas consumption	40	40	KFS

Table 6.1. CORAL budget

A Calculation of the muon momentum cut-off

A significant feature of the CORAL experiment is its depth of approximately 130 m, corresponding to a muon energy cutoff of approximately 70 GeV for vertical muons. This appendix reviews the results of detailed GEANT3 simulations of muon transport through the rock above the experimental region. These simulations include the effects of the major features of the experimental caverns as well as relevant surface structures. We present the muon energy cutoff as a function of zenith angle, as well as the muon energy spectrum in the experimental cavern based on a sample of 2000 extensive air showers generated using the CORSIKA Monte-Carlo and then evolved using the GEANT3 simulations to the cavern.

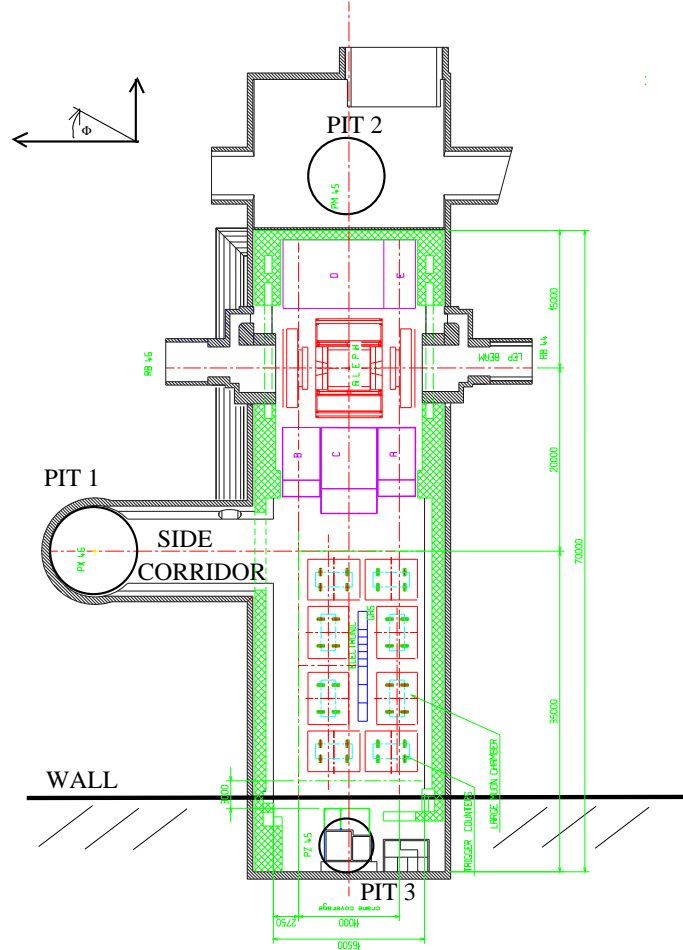


Figure A.1. Schematic View of the PA4 Cavern indicating the location of the three pits, the side corridor, and the wall on the surface.

The rock above PA4 is not uniform, but on average can be modelled by two layers of material: a 48 m thick slab of density of 2.2 g cm^{-3} , and a layer of molasse 77 m thick with a density of 2.5 g cm^{-3} . The geometry of the cavern at PA4 is illustrated in Fig. A.1. Six major geometrical elements are included in the simulation: the three vertical pits, the side corridor, the cylindrical experimental hall, and the 10 m high wall on the surface, which runs parallel to the beampipe [45].

The dependence of the muon energy cutoff on zenith angle, θ , was carefully studied. Samples of 300,000 muons with a flat momentum distribution and random azimuthal angle, Φ , were

generated for each zenith angle, $\theta = 0^\circ, 5^\circ, 10^\circ, \dots, 60^\circ$. All muons were located on the surface so as to point towards the center of the experimental apparatus. These muons were then evolved through the rock using the GEANT3 simulations.

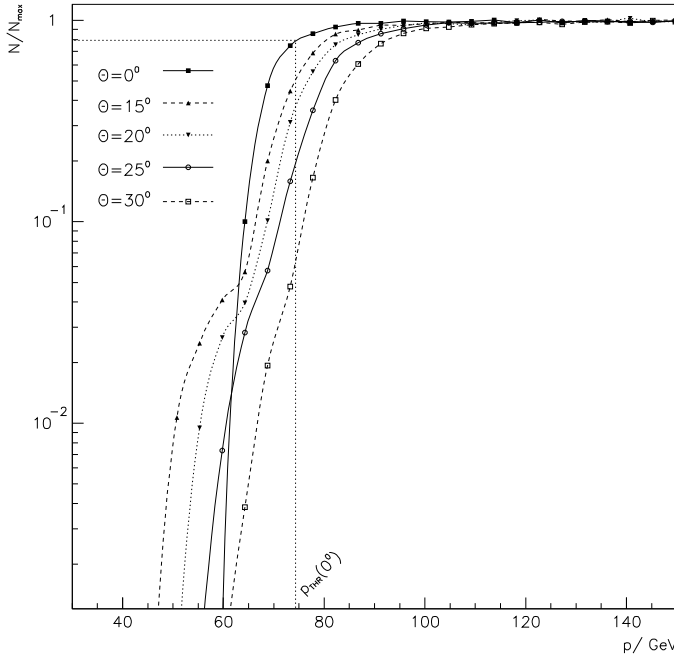


Figure A.2. Fraction of muons reaching the detector as a function initial muon momentum for several zenith angles, θ . The definition of the threshold momentum, p_{THR} , is illustrated for $\theta = 0^\circ$.

Fig. A.2 illustrates the results of these simulations. For small zenith angles, the spectrum is flat above 75 GeV, falling rapidly for lower energies. For larger zenith angles, small tails are apparent at low energies. These arise because some of the muons pass through the vertical tunnels and thus see less rock overburden than would otherwise be the case. This is clearly illustrated by Fig. A.3.

Fig. A.4 illustrates the dependence of the cutoff energy, taken to correspond to that momentum p_{THR} at which 80% of the initial muons make it through the rock to the experimental apparatus. The result climbs more steeply than the $1/\cos(\theta)$ one might naively expect due to simple geometric considerations. Indeed, this is largely due to the effects illustrated in Fig. A.3.

We have also studied the spectrum of muons reaching the experimental apparatus arising from cosmic ray induced air showers. A sample of 2000 extensive air showers arising from primary protons with energies in the range $1.0 \cdot 10^6 - 2.0 \cdot 10^7$ GeV were generated using CORSIKA [44]. These showers pointed to the center of the experimental apparatus. The energies at the surface of the muons from these showers reaching the experimental apparatus are shown in Fig. A.5.

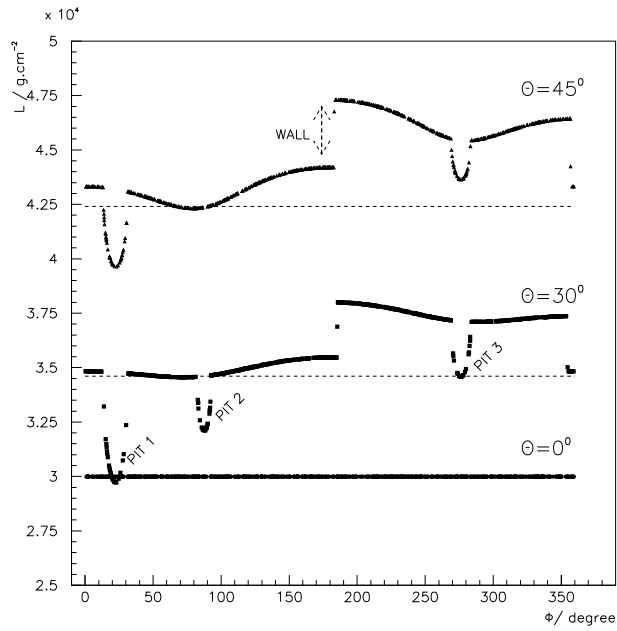


Figure A.3. The length of rock traversed by muons as a function of azimuthal angle Φ for three different zenith angles $\theta = 0^\circ, 15^\circ, 30^\circ$. The dashed lines represent the $L(0^\circ)/\cos(\theta)$ dependence discussed in the text.

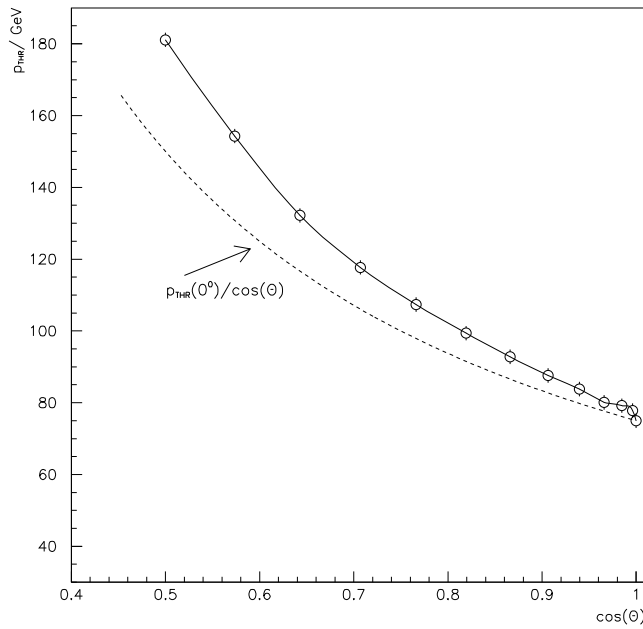


Figure A.4. Dependence of the muon threshold momentum p_{THR} as a function of zenith angle.

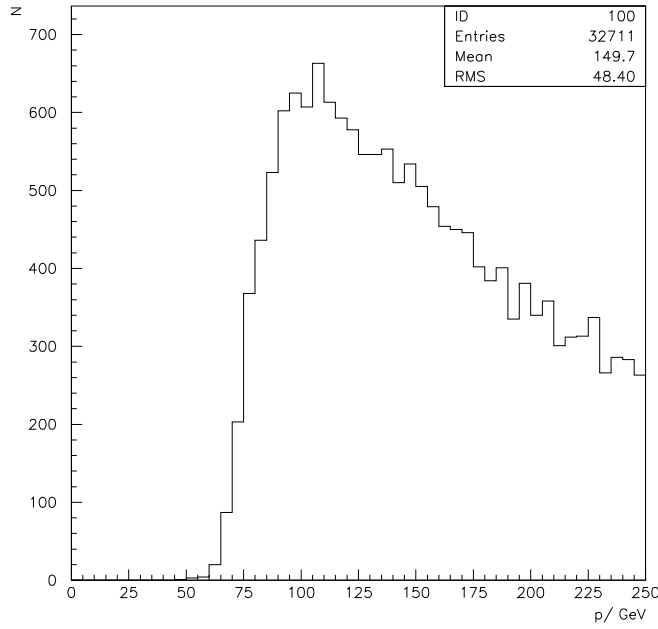


Figure A.5. Momentum spectrum of muons arising from air showers induced by protons with energies in the range $1.0 \cdot 10^6$ – $-2.0 \cdot 10^7$ GeV which reach the underground experimental apparatus. Note that the energies plotted are those of the muons at the surface.

Acknowledgements

It is a pleasure for us to thank the following people. Without their help this proposal would not have been possible. C. Antfolk, A. Besson, B. Betev, G. Beetham, P. Bonnal, C. Costa, M. Laakso, M. Poehler, J. Roche, E. Sabin, J. Sandstrom, J. Soulard, F. Terras, M. White, and J. Williamsson.

References

- [1] “*CosmoLep, an underground cosmic ray muon experiment in the LEP ring*”, CERN/LEPC 99-5, LEPC/P9.
- [2] MACRO Collaboration, M. Ambrosio et al., Phys. Rev. D **52**,(1995) 3793.
- [3] Y. Fukuda et al., Phys. Rev. Lett. 77, 1683 (1996), Phys. Rev. Lett 81, 1158 (1998), Phys. Lett B 433, 9 (1998).
- [4] R. Becker-Szendy et al., Nucl. Instr. Meth. A 324 (1993) 363-382.
- [5] Fréjus Collaboration, Ch. Berger et al., Phys. Rev. D **40**, 2163 (1989); Z. Phys. C – Particles and Fields **48**, 221 (1990).
- [6] Fréjus Collaboration, W. Rhode et al., Astropart. Phys. **4**, 217 (1996).
- [7] H.O. Klages for the KASCADE Collaboration, *Proc. 25th Int. Cosmic Ray Conference*, Durban (1997), Vol.8, 297
- [8] N. Chiba et al., Nucl. Instr. Meth. A 311 (1992) 338.
- [9] A. Borione et al., Nucl. Instr. Meth. A 346 (1994) 329.
- [10] Y. Hayashi et al. in Proceedings of the 26th Int. Cosmic Ray Conf., Salt Lake City, August 1999; Eds. D. B. Kieda et al; Vol 1, p. 276.

- [11] O.C. Allkofer, K. Eggert, P. Erhard et al. “*The UAI detector as a possible cosmic ray device*”, Proc. 17th Int. Cosmic Ray Conf., Paris, **10** (1981) 401
- [12] H. Wachsmuth, “*Proposal to search for Cosmic Ray coincidences in the LEP detectors* ” draft, 16.Dec.1993 (CosmoLEP-note 94.000)
A. Ball, G. Bonvicini,C. Grupen, et al. CERN/LEPC 94-10, LEPC/M 109 (1994)
- [13] P. Le Coultre, L3C collaboration, Proceedings of the 25th Int. Cosmic Ray Conf., Durban, South Africa, Vol. 7, p. 305.
“L3+Cosmics Experiment” in “Experiments at CERN in 1998” (Grey book), p.369.
- [14] “*Cosmic multi-muon events observed in the underground CERN-LEP tunnel with the ALEPH experiment*”, CERN EP/2000-152. Submitted to Astroparticle Physics.
- [15] B. Wiebel-Sooth, “*Measurement of all particle energy spectrum and chemical composition of cosmic rays with the HEGRA detector*” Dissertation, University Wuppertal, Sept 1998 WUB-DIS-98-9
- [16] ACCESS Formulation Study Report, NASA (2000, unpublished).
- [17] J. Hörandel for the KASCADE Collaboration, Proceedings of the 16th European Cosmic Ray Symposium, July 20-24, 1998, Dept. Fisica, Universidad de Alcala, Spain (ed: J. Medina) page 579.
- [18] D. Decamp et al., ALEPH Collaboration, NIM A **294** (1990) 121
- [19] E.V. Bugaev et al., Phys. Rev. D **58**,(1998) 1
- [20] SOUDAN Collaboration, Internal Report No. PDK-435, 1990 (unpublished).
- [21] S. M. Kasahara, Ph. D. thesis, University of Minnesota, 1995.
- [22] C. Castagnoli and O. Saavedra, Nuovo Cimento C **9**, 111 (1986).
- [23] NUSEX Collaboration, M. Aglietta et al., in *Proceedings of the Topical Seminar “Astrophysics and Particle Physics”*, San Miniato, Italy, 1989, edited by G. Castellini et al. [Nucl. Phys. B (Proc. Suppl.) **14B** (1990) 193].
- [24] N. Ito (for the KGF Collaboration), in *Proceedings of the International Symposium on Underground Physics Experiment*, Tokyo, Japan, 1990, edited by K. Nakamura (ICRR, Tokyo, 1990), p. 101.
- [25] Yu. M. Andreyev, V. I. Gurentsov, and I. M. Kogai, in *Proceedings of the 20th International Cosmic Ray Conference*, Moscow, USSR, August 2 – 15, 1987, edited by V. A. Koz-yarivsky et al. (Nauka, Moscow, 1987), Vol. **6**, p. 200.
- [26] Yu. M. Andreyev, A. E. Chudakov, V. I. Gurentsov, and I. M. Kogai, in *Proceedings of the 21st International Cosmic Ray Conference*, Adelaide, Australia, January 6 – 19, 1990, edited by R. J. Protheroe (Department of Physics and Mathematical Physics, University of Adelaide, Northfield, South Australia, 1990), Vol. **9**, p. 301; Yu. M. Andreyev (private communication).
- [27] LVD Collaboration, M. Aglietta et al., Astropart. Phys. **3**, 311 (1995).
- [28] V.N. Bakatanov et al., Physics of Atomic Nuclei, Vol. 61 No 9, (1998), 1507-1516.
- [29] Phys. Lett.**B267** (1991) 138-142.
- [30] Useful reviews include: K. Rajagopal, in *Quark-Gluon Plasma 2*, edited by R. Hwa, World Scientific, Singapore, (1995), p. 484; J-P. Blaizot and A. Krzywicki, Acta. Phys. Polon. B **27**, 1687 (1996); K. Ragjagopal, hep-ph/9703258, talk at the International Workshop on QCD Phase Transitions, January 1997, Hirschegg, Austria; J.D. Bjorken, in *Proceedings of the 1997 Zakopane School*, hep-ph/9712434.
- [31] J. J. Lord and J. Iwai, Paper 515, presented at the International Conference on High Energy Physics, Dallas (1992); H. Wilczynski et al., Proceedings of the XXIV International Cosmic Ray Conference, HE Sessions, Rome (1995), Vol.1, p.1.

- [32] J. Ridky, “*Can we observe the Quark Gluon Plasma in Cosmic Ray showers?*”, e-print archive hep-ph/0012068.
- [33] P.L. Biermann, T.K. Gaisser, T. Stanev Phys. Rev. D **51** (1995) 3450.
- [34] T.C. Weekes Space Sci. Rev. **59** (1992) 315.
- [35] F. Halzen, T. Stanev, G.B. Yodh MADPH 96-948, and astro-ph/9608201 and Phys. Rev. D **55** (1997) 4475.
- [36] F. Halzen, T. Stanev MADPH 95-901, astro-ph/9507362.
- [37] P. V. Ramanamurthy, A. W. Wolfendale *Gamma-ray Astronomy* Cambridge Astrophysics Series 1993
- [38] G.M. Samorski and W. Stamm, Ap. J. (Letters) 268, L17 (1983).
- [39] M. Marshak et al., Phys. Rev. Lett. 54, 2079 (1985) and Phys. Rev. Lett. 55, 1965 (1985); M.A. Thompson et al., Phys. Lett B 269, 220 (1991).
- [40] K. Eggert, Th. Ehlert, H. Faissner et al., NIM **176** (1980) 217
- [41] DELPHI Collaboration, Nucl. Instr. Meth. A303 (1991) 233.
- [42] W. Rhode *et al.* Nucl. Instr. Meth. A378 (1996) 399.
- [43] P. Billoir and Q. Qian, Nucl. Instr. and Meth., A294 (1990) 219.
- [44] D. Heck et al., Report **FZKA 6019** (1998), Forschungszentrum Karlsruhe J. Knapp, D. Heck, G. Schatz, Report **FZKA 5828** (1996), Forschungszentrum Karlsruhe
- [45] A.-S. Müller, diploma thesis, Mainz University, 1996